Engineering Analysis with Boundary Elements 36 (2012) 255–266

Contents lists available at ScienceDirect

Engineering Analysis with Boundary Elements

journal homepage: www.elsevier.com/locate/enganabound

A posteriori error estimates for the Johnson–Nédélec FEM–BEM coupling

M. Aurada, M. Feischl, M. Karkulik , D. Praetorius *

Institute for Analysis and Scientific Computing, Vienna University of Technology, Wiedner Hauptstraße 8-10, A-1040 Wien, Austria

ARTICLE INFO

Article history:
Received 25 February 2011
Accepted 27 July 2011
Available online 8 October 2011

Keywords:
Finite element-boundary element coupling
Local mesh-refinement
Adaptive algorithm

ABSTRACT

Only very recently, Sayas [The validity of Johnson–Nédélec's BEM-FEM coupling on polygonal interfaces. SIAM J Numer Anal 2009;47:3451–63] proved that the Johnson–Nédélec one-equation approach from [On the coupling of boundary integral and finite element methods. Math Comput 1980;35:1063–79] provides a stable coupling of finite element method (FEM) and boundary element method (BEM). In our work, we now adapt the analytical results for different a posteriori error estimates developed for the symmetric FEM–BEM coupling to the Johnson–Nédélec coupling. More precisely, we analyze the weighted-residual error estimator, the two-level error estimator, and different versions of $(h-h/2)$-based error estimators. In numerical experiments, we use these estimators to steer h-adaptive algorithms, and compare the effectivity of the different approaches.

1. Introduction

The FEM–BEM coupling is often used for interface problems in unbounded domains, where, e.g. non-linearities are present in a bounded domain and the material is isotropic in the exterior, cf. [22,24,36,34]. The symmetric FEM–BEM coupling was proposed and analyzed by Costabel [22] and attracted most attention in the mathematical literature. In engineering, however, more often the coupling procedure proposed by Johnson and Nédélec [37] is used since it only involves two integral operators instead of four. Only very recently, Sayas [46] proved that the Johnson–Nédélec coupling is well-posed even on polygonal domains, whereas numerical evidence of this was already known for many years, cf. e.g. [23].

To the best of our knowledge, the numerical analysis of a posteriori FEM–BEM error estimators has only been derived for the symmetric coupling. Most of the results follow the concept of two-level error estimation introduced in [42], see also the recent work [39] and the references therein. Other approaches include residual-based error estimators which have first been studied in [20], and recently also $(h-h/2)$-based error estimators [5].

In this work, we transfer these three classes of a posteriori error estimators from the symmetric coupling to the Johnson–Nédélec coupling. As model problem serves, for the ease of presentation, the interface problem for the Laplacian in two dimensions with an inhomogeneous volume force in the interior. We then formulate adaptive mesh-refining algorithms for each of these three approaches. In numerical experiments, we finally compare the effectiveness.

The detailed outline of this work reads as follows: In Section 2.1, we state our model problem and fix the notation of the integral operators involved. Section 2.2 introduces the Galerkin discretization and sketches the result of Sayas [46]. For some implementational reasons, we also discretize the given boundary data to which integral operators are applied. This allows to work with discrete integral operators, i.e. matrices, in the implementation and leads to some perturbed Galerkin formulation given in Section 2.3.

Section 3 is the heart of this work and contains the a posteriori error analysis. First, we collect the necessary notation in Sections 3.1 and 3.2. The a posteriori error control of the approximation error for the boundary data is discussed in Section 3.3. In Section 3.4, we study the residual error estimator ϱ_ℓ from [20]. In Section 3.5, we recall the $(h-h/2)$-error estimator μ_ℓ from [5] and discuss the so-called saturation assumption, whereas Section 3.6 is concerned with the two-level error estimator τ_ℓ from [42]. With certain modifications of the analysis from [5,20,42], we transfer these error estimators from the symmetric coupling to the Johnson–Nédélec coupling and can formulate and prove the according results. However, we stress that, first, our version of ϱ_ℓ is improved in the sense that it involves volume oscillations instead of the volume residual terms and, second, we also prove global equivalence $\mu_\ell \simeq \tau_\ell$ of $(h-h/2)$- and two-level error estimator. Finally, a short Section 3.7 provides local relations of τ_ℓ and ϱ_ℓ.

Section 4 considers an experiment from the literature for which uniform and adaptive mesh-refinement are compared with

* Corresponding author.
E-mail addresses: Markus.Aurada@tuwien.ac.at (M. Aurada), Michael.Feischl@tuwien.ac.at (M. Feischl), Michael.Karkulik@tuwien.ac.at (M. Karkulik), Dirk.Praetorius@tuwien.ac.at (D. Praetorius).
URLS: http://www.asc.tuwien.ac.at/~mkarkulik (M. Karkulik), http://www.asc.tuwien.ac.at/~dirk (D. Praetorius).

0955-7997
doi:10.1016/j.enganabound.2011.07.017

respect to empirical convergence rate and computational time. Finally, we conclude our work in Section 5 with an overview on the analytical and numerical results of this paper. Moreover, we state possible generalizations of our results for 3D problems and pose some questions for further research.

2. Johnson–Nédélec coupling

2.1. Model problem

We consider the linear interface problem

$$\begin{cases} -\Delta u^{\rm int} = f & \text{in } \Omega^{\rm int} := \Omega, \\ -\Delta u^{\rm ext} = 0 & \text{in } \Omega^{\rm ext} := \mathbb{R}^2\backslash\overline{\Omega}, \\ u^{\rm int} - u^{\rm ext} = u_0 & \text{on } \Gamma, \\ \partial_n u^{\rm int} - \partial_n u^{\rm ext} = \phi_0 & \text{on } \Gamma, \\ u^{\rm ext}(x) = \mathcal{O}(|x|^{-1}) & \text{as } |x|\to\infty. \end{cases} \tag{1}$$

Here, Ω is a bounded Lipschitz domain in $\mathbb{R}^2$ with boundary $\Gamma := \partial\Omega$ and exterior unit normal vector n. The given data satisfy $f \in L^2(\Omega)$, $u_0 \in H^{1/2}(\Gamma)$, and $\phi_0 \in H^{-1/2}(\Gamma)$. The space $H^{1/2}(\Gamma)$ is precisely the space of all traces of functions from $H^1(\Omega)$, and $H^{-1/2}(\Gamma)$ is the dual of $H^{1/2}(\Gamma)$ with respect to the extended $L^2(\Gamma)$-scalar product. To guarantee the solvability of (1), we need the data to satisfy $\langle \phi_0, 1\rangle_\Gamma + \langle f, 1\rangle_\Omega = 0$. As usual, (1) is understood in the weak sense, and the sought solutions satisfy $u^{\rm int} \in H^1(\Omega)$ and $u^{\rm ext} \in H^1_{\ell oc}(\Omega^{\rm ext}) = \{v : \Omega^{\rm ext} \to \mathbb{R} : \forall K \subset \Omega^{\rm ext} \text{ compact } v \in H^1(K)\}$ with $\nabla u^{\rm ext} \in L^2(\Omega^{\rm ext})$.

Problem (1) is equivalently stated via the Johnson–Nédélec FEM–BEM coupling proposed in [37]: Find $\mathbf{u} := (u,\phi) \in \mathcal{H} := H^1(\Omega^{\rm int}) \times H^{-1/2}(\Gamma)$ such that

$$\begin{aligned} &\langle \nabla u, \nabla v\rangle_\Omega - \langle \phi, v\rangle_\Gamma = \langle f, v\rangle_\Omega + \langle \phi_0, v\rangle_\Gamma \quad \text{for all } v \in H^1(\Omega^{\rm int}), \\ &\langle \psi, (\tfrac12 - \mathfrak{K})u + \mathfrak{V}\phi\rangle_\Gamma = \langle \psi, (\tfrac12 - \mathfrak{K})u_0\rangle_\Gamma \quad \text{for all } \psi \in H^{-1/2}(\Gamma). \end{aligned} \tag{2}$$

Here, $\mathfrak{V}$ denotes the simple-layer potential and $\mathfrak{K}$ denotes the double-layer potential. With

$$G(z) := -\frac{1}{2\pi}\log|z| \quad \text{for } z \in \mathbb{R}^2\backslash\{0\} \tag{3}$$

the fundamental solution of the 2D Laplacian, these integral operators formally read for $x \in \Gamma$ as follows:

$$(\mathfrak{V}\psi)(x) = \int_\Gamma G(x-y)\psi(y)\, d\Gamma(y), \tag{4}$$

$$(\mathfrak{K}v)(x) = \int_\Gamma \partial_{n(y)} G(x-y) v(y)\, d\Gamma(y). \tag{5}$$

By continuous extension, these definitions provide linear boundary integral operators $\mathfrak{V} \in L(H^{-1/2}(\Gamma); H^{1/2}(\Gamma))$ and $\mathfrak{K} \in L(H^{1/2}(\Gamma); H^{1/2}(\Gamma))$. By scaling of Ω, we may assume that $\operatorname{diam}(\Omega) < 1$ to ensure the uniform ellipticity of $\mathfrak{V}$, i.e.

$$\|\psi\|^2_{H^{-1/2}(\Gamma)} \lesssim \langle \psi, \mathfrak{V}\psi\rangle_\Gamma \quad \text{for all } \psi \in H^{-1/2}(\Gamma).$$

In particular, $\langle \phi, \psi\rangle_{\mathfrak{V}} := \langle \phi, \mathfrak{V}\psi\rangle_\Gamma$ is a scalar product, and

$$\|\psi\|^2_{\mathfrak{V}} := \langle \psi, \mathfrak{V}\psi\rangle_\Gamma \quad \text{for } \psi \in H^{-1/2}(\Gamma)$$

defines an equivalent norm on $H^{-1/2}(\Gamma)$. The reader is referred to e.g. [41] for proofs and further details on these integral operators. The link between (1) and (2) is provided by $u = u^{\rm int}$ and $\phi = \partial_n u^{\rm ext}$, and $u^{\rm ext}$ is then given by the third Green's formula

$$u^{\rm ext}(x) = \tilde{\mathfrak{K}}(u-u_0)(x) - \tilde{\mathfrak{V}}\phi(x) \quad \text{for } x \in \Omega^{\rm ext}, \tag{6}$$

where the potentials $\tilde{\mathfrak{V}}$ and $\tilde{\mathfrak{K}}$ formally denote the operators $\mathfrak{V}$ and $\mathfrak{K}$, but are now evaluated in $\Omega^{\rm ext}$ instead of Γ. Note carefully that we do not use a notational difference for the function $u \in H^1(\Omega)$ and its trace $u \in H^{1/2}(\Gamma)$, for which we compute the boundary integral $(\frac12 - \mathfrak{K})u$ in (2).

We stress that the second equation of the Johnson–Nédélec FEM–BEM coupling (2) is the same as for the mathematically well-studied symmetric coupling. It has already been proved in [37] that problem (2) is well-posed on the continuous level, i.e. it admits a unique solution $\mathbf{u} = (u,\phi) \in \mathcal{H}$.

2.2. Galerkin discretization

Let $\mathcal{T}_\ell$ be a regular triangulation of Ω into triangles $T_j \in \mathcal{T}_\ell$ and $\mathcal{E}^\Gamma_\ell$ a partition of the coupling boundary Γ into piecewise affine line segments $E_j \in \mathcal{E}^\Gamma_\ell$. Throughout, the index $\ell \in \mathbb{N}_0$ indicates the current step of the adaptive loop considered below. We use a conforming discretization with continuous and $\mathcal{T}_\ell$-piecewise affine finite elements in Ω and $\mathcal{E}^\Gamma_\ell$-piecewise constants on Γ, i.e. the discrete spaces read

$$\mathcal{X}_\ell := \mathcal{S}^1(\mathcal{T}_\ell) \times \mathcal{P}^0(\mathcal{E}^\Gamma_\ell) \subset H^1(\Omega) \times H^{-1/2}(\Gamma) = \mathcal{H}. \tag{7}$$

We stress that our analysis does not enforce any coupling of $\mathcal{E}^\Gamma_\ell$ and $\mathcal{T}_\ell$. However, for the ease of presentation and implementation, we will assume throughout that the boundary mesh $\mathcal{E}^\Gamma_\ell = \mathcal{T}_\ell|_\Gamma$ is obtained by restriction of the triangulation $\mathcal{T}_\ell$ to the boundary Γ.

The Galerkin formulation of (2) then reads as follows: Find $\mathbf{U}^\star_\ell := (U^\star_\ell, \Phi^\star_\ell) \in \mathcal{X}_\ell$ such that

$$\begin{aligned} &\langle \nabla U^\star_\ell, \nabla V_\ell\rangle_\Omega - \langle \Phi^\star_\ell, V_\ell\rangle_\Gamma = \langle f, V_\ell\rangle_\Omega + \langle \phi_0, V_\ell\rangle_\Gamma, \\ &\langle \Psi_\ell, (\tfrac12 - \mathfrak{K})U^\star_\ell + \mathfrak{V}\Phi^\star_\ell\rangle_\Gamma = \langle \Psi_\ell, (\tfrac12 - \mathfrak{K})u_0\rangle_\Gamma \end{aligned} \tag{8}$$

for all $\mathbf{V}_\ell := (V_\ell, \Psi_\ell) \in \mathcal{X}_\ell$. Only very recently [46, Theorem 2], it has been proven that the discrete formulation (8) is well-posed and admits a unique Galerkin solution $\mathbf{U}^\star_\ell \in \mathcal{X}_\ell$. We stress that the following result applies, in particular, also to the continuous formulation (2) and provides an alternate proof for the existence and uniqueness of a solution of the Johnson–Nédélec FEM–BEM coupling.

Proposition 1 (*Sayas [46]*). *Suppose that X_ℓ is a closed subspace of $H^1(\Omega)$ and Y_ℓ is a closed subspace of $H^{-1/2}(\Gamma)$ which satisfy*

$$1 \in X_\ell \quad \text{as well as} \quad 1 \in Y_\ell, \tag{9}$$

i.e. the discrete spaces contain the constant functions. With $\mathcal{X}_\ell := X_\ell \times Y_\ell$, the linear operator $\mathbb{H} : \mathcal{X}_\ell \to \mathcal{X}_\ell^*$

$$\begin{aligned} (\mathbb{H}\mathbf{U}_\ell)(\mathbf{V}_\ell) := {} & \langle \nabla U_\ell, \nabla V_\ell\rangle_\Omega - \langle \Phi_\ell, V_\ell\rangle_\Gamma \\ & + \langle \Psi_\ell, (\tfrac12 - \mathfrak{K})U_\ell + \mathfrak{V}\Phi_\ell\rangle_\Gamma \end{aligned} \tag{10}$$

for $\mathbf{U}_\ell = (U_\ell, \Phi_\ell)$, $\mathbf{V}_\ell = (V_\ell, \Psi_\ell) \in \mathcal{X}_\ell$ defines an isomorphism, where the bounds of the operator norms $\|\mathbb{H}\|$ and $\|\mathbb{H}^{-1}\|$ depend only on Ω, but not on the chosen spaces X_ℓ and Y_ℓ. In particular, the variational form (8) admits a unique solution $\mathbf{U}^\star_\ell \in \mathcal{X}_\ell$. Moreover, there holds the Céa-type quasi-optimality

$$|||\mathbf{u} - \mathbf{U}^\star_\ell||| \le C_{\rm opt} \min_{\mathbf{V}_\ell \in \mathcal{X}_\ell} |||\mathbf{u} - \mathbf{V}_\ell||| \tag{11}$$

with $|||\mathbf{v}|||^2 := \|v\|^2_{H^1(\Omega)} + \|\psi\|^2_{\mathfrak{V}}$ for $\mathbf{v} = (v,\psi) \in \mathcal{H}$, and the constant $C_{\rm opt} > 0$ depends only on Ω, but not on $\mathcal{X}_\ell$ or the given data f, ϕ_0, and u_0.

2.3. Perturbed Galerkin discretization

The right-hand side of (8) involves the evaluation of $\mathfrak{K}u_0$, which can be computed by methods proposed in [19,44,45]. In this work, we will follow another approach. We propose to approximate at least the given trace data $u_0 \in H^{1/2}(\Gamma)$ by appropriate discrete functions. One reason for this is that so-called *fast methods for boundary integral operators* usually deal with discrete

functions, cf. [43]. Another reason for this, which is related with the question of convergence of adaptive methods, is discussed at the end of Section 5.4. Following [5,6], we assume additional regularity $u_0 \in H^1(\Gamma)$, and consider the nodal interpolant

$$U_{0,\ell} := I_\ell u_0 = \sum_{j=1}^{n} u_0(z_j)\zeta_j \in \mathcal{S}^1(\mathcal{E}_\ell^\Gamma), \tag{12}$$

where $z_j \in \Gamma$ denotes a node of $\mathcal{E}_\ell^\Gamma$ and where ζ_j is the associated $\mathcal{E}_\ell^\Gamma$-piecewise linear and continuous hat function, i.e. $\zeta_j(z_k) = \delta_{jk}$. Now, the perturbed Galerkin formulation reads as follows: Find $\mathbf{U}_\ell := (U_\ell, \Phi_\ell) \in \mathcal{X}_\ell$ such that

$$\begin{aligned} &\langle \nabla U_\ell, \nabla V_\ell \rangle_\Omega - \langle \Phi_\ell, V_\ell \rangle_\Gamma = \langle f, V_\ell \rangle_\Omega + \langle \phi_0, V_\ell \rangle_\Gamma, \\ &\langle \Psi_\ell, (\tfrac{1}{2} - \mathfrak{K}) U_\ell + \mathfrak{V} \Phi_\ell \rangle_\Gamma = \langle \Psi_\ell, (\tfrac{1}{2} - \mathfrak{K}) U_{0,\ell} \rangle_\Gamma, \end{aligned} \tag{13}$$

for all $(V_\ell, \Psi_\ell) \in \mathcal{X}_\ell$. Compared to (8), the only difference is that (13) involves the approximate data $U_{0,\ell}$ instead of u_0 on the right-hand side. Consequently, Proposition 1 applies and proves that (13) has a unique solution $\mathbf{U}_\ell \in \mathcal{X}_\ell$.

3. A posteriori error control

3.1. Notation

Let $\mathcal{T}_\ell$ be a regular triangulation of Ω into triangles which is obtained by adaptive local refinement of an initial triangulation $\mathcal{T}_0$. Then, $\mathcal{E}_\ell^\Gamma = \mathcal{T}_\ell|_\Gamma$ denotes the induced partition of Γ, i.e. the set of all boundary edges. Let $\mathcal{E}_\ell^\Omega$ denote the set of all edges of the volume triangulation $\mathcal{T}_\ell$ which lie inside Ω, i.e. for $E \in \mathcal{E}_\ell^\Omega$ exist unique elements $T_+, T_- \in \mathcal{T}_\ell$ with $E = T_+ \cap T_-$. We then denote the corresponding edge patch by $\omega_{\ell,E} := T_+ \cup T_-$. Furthermore, we denote by $\mathcal{K}_\ell$ the set of nodes of $\mathcal{T}_\ell$. For $z \in \mathcal{K}_\ell$, denote by $\mathcal{E}_{\ell,z}$ the set of all edges $E' \in \mathcal{E}_\ell^\Omega \cup \mathcal{E}_\ell^\Gamma$ which have z as a node.

To exclude some pathological cases, we restrict ourselves to meshes $\mathcal{T}_\ell$ which meet the following conditions:

- each element $T \in \mathcal{T}_\ell$ has at most one edge on the boundary Γ,
- each interior edge $E \in \mathcal{E}_\ell^\Omega$ has at most one node on the boundary Γ.

We stress that these assumptions are essentially conditions on the initial triangulation $\mathcal{T}_0$.

Let $\mathrm{diam}(\omega)$ denote the Euclidean diameter of a set $\omega \subset \mathbb{R}^2$. For $x \in \tau \in \mathcal{T}_\ell \cup \mathcal{E}_\ell^\Gamma$, we define the local mesh-width function by $h_\ell(x) := \mathrm{diam}(\tau)$. This definition provides functions $h_\ell \in L^\infty(\Omega)$ as well as $h_\ell \in L^\infty(\Gamma)$ and $h_\ell \in L^\infty(\bigcup \mathcal{E}_\ell^\Omega)$, where $\bigcup \mathcal{E}_\ell^\Omega$ denotes the interior skeleton of $\mathcal{T}_\ell$.

3.2. Local mesh-refinement

For the local refinement of the volume mesh $\mathcal{T}_\ell$, we use newest vertex bisection with the following conventions, cf. Fig. 1: for marked triangles, we mark all three edges, and all marked edges are bisected. We refer to [49, Chapter 5] for details on newest vertex bisection. By others, this mesh-refinement ensures uniform shape regularity of $\mathcal{T}_\ell$. More precisely, the shape regularity constant

$$\sigma(\mathcal{T}_\ell) := \max\{\mathrm{diam}(T)^2/|T| : T \in \mathcal{T}_\ell\} \tag{14}$$

depends only on the initial mesh $\mathcal{T}_0$, i.e.

$$\sup_{\ell \in \mathbb{N}} \sigma(\mathcal{T}_\ell) \le C\, \sigma(\mathcal{T}_0), \tag{15}$$

where $C > 0$ depends only on the labeling of the reference edges in $\mathcal{T}_0$. Marking of an element $E \in \mathcal{E}_\ell^\Gamma = \mathcal{T}_\ell|_\Gamma$ means marking of certain edges of some triangles $T \in \mathcal{T}_\ell$ for newest vertex bisection. We stress that this guarantees that marked edges E are split into two sons of half length. Moreover, due to uniform shape regularity (15) of $\mathcal{T}_\ell$, there automatically holds

$$\sup_{\ell \in \mathbb{N}} \kappa(\mathcal{E}_\ell^\Gamma) \le C\, \kappa(\mathcal{E}_0^\Gamma) \tag{16}$$

for the K-mesh constant (or: local mesh-ratio)

$$\kappa(\mathcal{E}_\ell^\Gamma) := \max\{\mathrm{diam}(E)/\mathrm{diam}(E') : E, E' \in \mathcal{E}_\ell^\Gamma \text{ with } E \cap E' \neq \emptyset\}, \tag{17}$$

and the constant $C > 0$ depends only on $\mathcal{T}_0$. Finally, there holds nestedness $\mathcal{S}^1(\mathcal{T}_\ell) \subseteq \mathcal{S}^1(\mathcal{T}_{\ell+1})$, $\mathcal{P}^0(\mathcal{E}_\ell^\Gamma) \subseteq \mathcal{P}^0(\mathcal{E}_{\ell+1}^\Gamma)$ whence consequently $\mathcal{X}_\ell \subseteq \mathcal{X}_{\ell+1}$.

3.3. Error control of data approximation

In the following, we consider a continuous auxiliary problem, where the right-hand side is given as in (13): Find $\mathbf{u}_\ell := (u_\ell, \phi_\ell) \in \mathcal{H}$ such that

$$\begin{aligned} &\langle \nabla u_\ell, \nabla v \rangle_\Omega - \langle \phi_\ell, v \rangle_\Gamma = \langle f, v \rangle_\Omega + \langle \phi_0, v \rangle_\Gamma, \\ &\langle \psi, (\tfrac{1}{2} - \mathfrak{K}) u_\ell + \mathfrak{V} \phi_\ell \rangle_\Gamma = \langle \psi, (\tfrac{1}{2} - \mathfrak{K}) U_{0,\ell} \rangle_\Gamma \end{aligned} \tag{18}$$

for all $\mathbf{v} = (v, \psi) \in \mathcal{H}$. By definition, $\mathbf{U}_\ell \in \mathcal{X}_\ell$ then is a Galerkin approximation of $\mathbf{u}_\ell \in \mathcal{H}$ so that the quasi-optimality (11) holds with $\mathbf{u}$ and $\mathbf{U}_\ell^\star$ replaced by $\mathbf{u}_\ell$ and $\mathbf{U}_\ell$, respectively.

For the symmetric FEM–BEM coupling for some non-linear interface problem, the following result is already stated in [5, Proposition 1]:

Proposition 2. *With $\mathbf{u}, \mathbf{u}_\ell \in \mathcal{H}$ the continuous solutions of (2) and (18) and $\mathbf{U}_\ell^\star, \mathbf{U}_\ell \in \mathcal{X}_\ell$ the corresponding Galerkin solutions of (8) and (13), it holds*

$$C_1^{-1} \|\mathbf{U}_\ell^\star - \mathbf{U}_\ell\| \le \|\mathbf{u} - \mathbf{u}_\ell\| \le C_2\, \mathrm{osc}_{\Gamma,\ell} \quad \text{with } \mathrm{osc}_{\Gamma,\ell} := \|h_\ell^{1/2}(u_0 - U_{0,\ell})'\|_{L^2(\Gamma)}, \tag{19}$$

where $(\cdot)'$ denotes the arclength derivative along Γ. While $C_1 > 0$ depends only on Ω, the constant $C_2 > 0$ depends additionally on $\sigma(\mathcal{T}_0)$.

Proof. According to linearity, $\mathbf{U}_\ell^\star - \mathbf{U}_\ell \in \mathcal{X}_\ell$ is the Galerkin approximation of $\mathbf{u} - \mathbf{u}_\ell \in \mathcal{H}$. Therefore, the quasi-optimality (11) proves

$$\|\mathbf{U}_\ell^\star - \mathbf{U}_\ell\| \le \|(\mathbf{u} - \mathbf{u}_\ell) - (\mathbf{U}_\ell^\star - \mathbf{U}_\ell)\| + \|\mathbf{u} - \mathbf{u}_\ell\| \lesssim \|\mathbf{u} - \mathbf{u}_\ell\|.$$

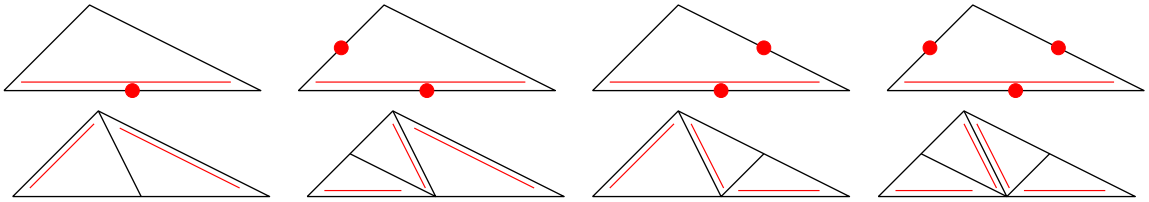

Fig. 1. For each triangle $T \in \mathcal{T}_\ell$, there is one fixed *reference edge*, indicated by the double line (left, top). Refinement of T is done by bisecting the reference edge, where its midpoint becomes a new node. The reference edges of the son triangles $T' \in \mathcal{T}_{\ell+1}$ are opposite to this newest vertex (left, bottom). To avoid hanging nodes, one proceeds as follows: We assume that certain edges of T, but at least the reference edge, are marked for refinement (top). Using iterated newest vertex bisection, the element is then split into 2, 3, or 4 son triangles (bottom).

Recall that the linear mapping $\mathbb{H}:\mathcal{H}\to\mathcal{H}^*$ from (10) is an isomorphism. Therefore, there holds

$$|||\mathbf{u}-\mathbf{u}_\ell||| \simeq \|\mathbb{H}\mathbf{u}-\mathbb{H}\mathbf{u}_\ell\|_{\mathcal{H}^*} \simeq \|u_0-U_{0,\ell}\|_{H^{1/2}(\Gamma)}$$

since only the trace data differ. By definition, there holds $u_0-U_{0,\ell}=(1-I_\ell)u_0$. Nodal interpolation on the one-dimensional manifold Γ satisfies

$$C_3^{-1}\|v-I_\ell v\|_{H^{1/2}(\Gamma)} \le \|h_\ell^{1/2}(v-I_\ell v)'\|_{L^2(\Gamma)} \le \|h_\ell^{1/2}v'\|_{L^2(\Gamma)} \quad \text{for all } v\in H^1(\Gamma), \tag{20}$$

see [12, Theorem 1; 16, Corollary 3.4; 28, Lemma 2.2], where the constant $C_3>0$ depends only on Γ and an upper bound of the local mesh-ratio $\kappa(\mathcal{E}_\ell^\Gamma)$. □

3.4. Residual-based error estimator

Let $[\partial_n U_\ell]|_E$ denote the jump of $\partial_n U_\ell$ over the edge $E\in\mathcal{E}_\ell^\Omega$. We assume additional regularity $\phi_0\in L^2(\Gamma)$ for the given data and define the edge jump contributions by

$$\gamma_\ell^2 := \sum_{E\in\mathcal{E}_\ell^\Omega}\gamma_\ell(E)^2 \quad \text{with } \gamma_\ell(E) := \|h_\ell^{1/2}[\partial_n U_\ell]\|_{L^2(E)}$$

as well as the edge oscillations by

$$\mathrm{osc}_{\Omega,\ell}^2 := \sum_{E\in\mathcal{E}_\ell^\Omega}\mathrm{osc}_{\Omega,\ell}(E)^2 \quad \text{with } \mathrm{osc}_{\Omega,\ell}(E) := \|h_\ell(f-f_E)\|_{L^2(\omega_{\ell,E})},$$

where $f_E=|\omega_{\ell,E}|^{-1}\int_{\omega_{\ell,E}} f\,dx$ denotes the integral mean of f over $\omega_{\ell,E}$.

Lemma 3. *The following local estimates hold*:

(i) $\mathrm{osc}_{\Omega,\ell}(E)\le C_4\|h_\ell f\|_{L^2(\omega_{\ell,E})}$ *for all* $E\in\mathcal{E}_\ell^\Omega$,
(ii) $\|h_\ell f\|_{L^2(T)}\le C_5(\gamma_\ell(\mathcal{E}_{\ell,z})+\mathrm{osc}_{\Omega,\ell}(\mathcal{E}_{\ell,z}))$ *for all* $z\in(\mathcal{K}_\ell\cap T)\backslash\Gamma$,

where we abbreviate e.g. $\gamma_\ell(\mathcal{E}_{\ell,z})^2=\sum_{E\in\mathcal{E}_{\ell,z}}\gamma_\ell(E)^2$. *The constants* $C_4,C_5>0$ *depend only on the shape regularity* $\sigma(\mathcal{T}_0)$ *of the initial mesh.*

Proof. The first estimate follows by the best approximation property of f_E. The proof of the second estimate is found e.g. in [33, Lemma 4] and relies on certain inverse-type estimates as well as on the fact that newest vertex bisection only leads to finitely many shapes of triangles. □

We now have the following reliability result for a residual-based a posteriori error estimate.

Theorem 4. *Suppose that* $\mathbf{u}_\ell\in\mathcal{H}$ *is the unique solution of* (18) *and* $\mathbf{U}_\ell\in\mathcal{X}_\ell$ *is its Galerkin approximation* (13). *Assume additional regularity* $\phi_0\in L^2(\Gamma)$. *Then, there holds*

$$C_6^{-1}|||\mathbf{u}_\ell-\mathbf{U}_\ell||| \le \varrho_\ell := (\mathrm{osc}_{\Omega,\ell}^2+\gamma_\ell^2+\|h_\ell^{1/2}(\phi_0+\Phi_\ell-\partial_n U_\ell)\|_{L^2(\Gamma)}^2 + \|h_\ell^{1/2}((\tfrac12-\mathfrak{K})(U_{0,\ell}-U_\ell)-\mathfrak{V}\Phi_\ell)'\|_{L^2(\Gamma)}^2)^{1/2}, \tag{21}$$

where the constant $C_6>0$ *depends only on* Ω *and* $\sigma(\mathcal{T}_0)$.

Proof. We consider the isomorphism $\mathbb{H}:\mathcal{H}\to\mathcal{H}^*$ from (10) and the functional $F_\ell\in\mathcal{H}^*$ defined by

$$F_\ell(\mathbf{v}) := \langle f,v\rangle_\Omega+\langle\phi_0,v\rangle_\Gamma+\langle\psi,(\tfrac12-\mathfrak{K})U_{0,\ell}\rangle_\Gamma \quad \text{for } \mathbf{v}=(v,\psi)\in\mathcal{H}. \tag{22}$$

Note that (18) is equivalently stated by

$$(\mathbb{H}\mathbf{u}_\ell)(\mathbf{v})=F_\ell(\mathbf{v}) \quad \text{for all } \mathbf{v}\in\mathcal{H},$$

whereas the Galerkin (13) reads

$$(\mathbb{H}\mathbf{U}_\ell)(\mathbf{V}_\ell)=F_\ell(\mathbf{V}_\ell) \quad \text{for all } \mathbf{V}_\ell\in\mathcal{X}_\ell.$$

This and the fact that $\mathbb{H}$ is an isomorphism yields

$$|||\mathbf{u}_\ell-\mathbf{U}_\ell||| \simeq \sup_{\mathbf{v}\in\mathcal{H}\backslash\{0\}}\frac{|F_\ell(\mathbf{v})-\mathbb{H}\mathbf{U}_\ell(\mathbf{v})|}{|||\mathbf{v}|||} = \sup_{\mathbf{v}\in\mathcal{H}\backslash\{0\}}\frac{|F_\ell(\mathbf{v}-\mathbf{V}_\ell)-\mathbb{H}\mathbf{U}_\ell(\mathbf{v}-\mathbf{V}_\ell)|}{|||\mathbf{v}|||} \tag{23}$$

for all $\mathbf{V}_\ell\in\mathcal{X}_\ell$. To estimate the right-hand side, let $\mathbf{v}=(v,\psi)\in\mathcal{H}$ and $\mathbf{V}_\ell=(J_\ell v,0)\in\mathcal{X}_\ell$, where $J_\ell:H^1(\Omega)\to\mathcal{S}^1(\mathcal{T}_\ell)$ is a Clément-type quasi-interpolation operator, see e.g. [1,49]. Note that

$$\begin{aligned}F_\ell(\mathbf{v}-\mathbf{V}_\ell)-\mathbb{H}\mathbf{U}_\ell(\mathbf{v}-\mathbf{V}_\ell) &= \langle f,v-J_\ell v\rangle_\Omega-\langle\nabla U_\ell,\nabla(v-J_\ell v)\rangle_\Omega\\ &\quad+\langle\phi_0+\Phi_\ell,v-J_\ell v\rangle_\Gamma\\ &\quad+\langle\psi,(\tfrac12-\mathfrak{K})(U_{0,\ell}-U_\ell)-\mathfrak{V}\Phi_\ell\rangle_\Gamma.\end{aligned} \tag{24}$$

With standard arguments [1,49], we infer

$$\begin{aligned}&|F_\ell(\mathbf{v}-\mathbf{V}_\ell)-\mathbb{H}\mathbf{U}_\ell(\mathbf{v}-\mathbf{V}_\ell)|\\ &\quad\lesssim \|v\|_{H^1(\Omega)}\|h_\ell f\|_{L^2(\Omega)}+\|v\|_{H^1(\Omega)}\|h_\ell^{1/2}[\partial_n U_\ell]\|_{L^2(\bigcup\mathcal{E}_\ell^\Omega)}\\ &\qquad+\|v\|_{H^1(\Omega)}\|h_\ell^{1/2}(\phi_0+\Phi_\ell-\partial_n U_\ell)\|_{L^2(\Gamma)}\\ &\qquad+\|\psi\|_{H^{-1/2}(\Gamma)}\|(\tfrac12-\mathfrak{K})(U_{0,\ell}-U_\ell)-\mathfrak{V}\Phi_\ell\|_{H^{1/2}(\Gamma)}\\ &\quad\le |||\mathbf{v}|||(\|h_\ell f\|_{L^2(\Omega)}+\gamma_\ell+\|h_\ell^{1/2}(\phi_0+\Phi_\ell-\partial_n U_\ell)\|_{L^2(\Gamma)}\\ &\qquad+\|(\tfrac12-\mathfrak{K})(U_{0,\ell}-U_\ell)-\mathfrak{V}\Phi_\ell\|_{H^{1/2}(\Gamma)}).\end{aligned} \tag{25}$$

With Lemma 3, we see

$$\|h_\ell f\|_{L^2(\Omega)}\lesssim \mathrm{osc}_{\Omega,\ell}+\gamma_\ell.$$

Finally, it remains to estimate the last term in (25). To this end, we need the following 2D BEM result from [12, Theorem 1], see also [29,47]: *Provided that the function* $w\in H^1(\Gamma)$ *has at least one zero on each element* $E\in\mathcal{E}_\ell^\Gamma$, *there holds*

$$\|w\|_{H^{1/2}(\Gamma)}\le C_7\|h_\ell^{1/2}w'\|_{L^2(\Gamma)}, \tag{26}$$

where the constant $C_7>0$ *depends only on* Γ *and an upper bound of* $\kappa(\mathcal{E}_\ell^\Gamma)$. We apply this result to $w:=(\frac12-\mathfrak{K})(U_{0,\ell}-U_\ell)-\mathfrak{V}\Phi_\ell$. First, note that $U_{0,\ell}-U_\ell\in H^1(\Gamma)$. Second, note that $\Phi_\ell\in L^2(\Gamma)$. Third, recall that $\mathfrak{V}:H^{s-1/2}(\Gamma)\to H^{s+1/2}(\Gamma)$ and $\mathfrak{K}:H^{s+1/2}(\Gamma)\to H^{s+1/2}(\Gamma)$ are bounded linear operators for all $-1/2\le s\le 1/2$. Consequently, the case $s=1/2$ proves $w\in H^1(\Gamma)$, and the Sobolev inequality on one-dimensional manifolds implies that w is continuous. Due to the second equality in (13), we see that

$$\int_E w\,d\Gamma=0 \quad \text{for all } E\in\mathcal{E}_\ell^\Gamma,$$

where we simply choose $\Psi_\ell=\chi_E\in\mathcal{P}^0(\mathcal{E}_\ell^\Gamma)$ to be a characteristic function. Consequently, the continuous function w has at least one zero on each $E\in\mathcal{E}_\ell^\Gamma$. Now, [12, Theorem 1] yields

$$\|(\tfrac12-\mathfrak{K})(U_{0,\ell}-U_\ell)-\mathfrak{V}\Phi_\ell\|_{H^{1/2}(\Gamma)}\lesssim\|h_\ell^{1/2}((\tfrac12-\mathfrak{K})(U_{0,\ell}-U_\ell)-\mathfrak{V}\Phi_\ell)'\|_{L^2(\Gamma)}.$$

This concludes the proof of (21). □

Due to the triangle inequality and the aforegoing propositions, we have the following result.

Corollary 5. *Suppose that* $\mathbf{u}\in\mathcal{H}$ *is the solution of* (2), *whereas* $\mathbf{U}_\ell\in\mathcal{X}_\ell$ *solves the perturbed Galerkin scheme* (13). *Then,*

$$C_8^{-1}|||\mathbf{u}-\mathbf{U}_\ell|||\le\overline{\varrho}_\ell := (\varrho_\ell^2+\mathrm{osc}_{\Gamma,\ell}^2)^{1/2}, \tag{27}$$

where $\mathrm{osc}_{\Gamma,\ell}$ *and* ϱ_ℓ *are defined in Proposition 2 and Theorem 4. The constant* $C_8>0$ *depends only on* Ω *and* $\sigma(\mathcal{T}_0)$. □

3.5. (h−h/2)-type error estimator

In [5], we recently introduced some simple $(h-h/2)$-based error estimators for the symmetric FEM–BEM coupling. The $(h-h/2)$-error estimation strategy is a well-known technique for the a posteriori estimation of the error in the energy norm $|||\mathbf{u}-\mathbf{U}_\ell|||$; see [35] in the context of ordinary differential

equations, and the works of Bank [7–9] or the monograph [1, Chapter 5] in the context of the finite element method.

Suppose that $\mathbf{U}_\ell \in \mathcal{X}_\ell$ is the Galerkin solution (13) for some given mesh $\mathcal{T}_\ell$. Let $\widehat{\mathcal{T}}_\ell$ be the uniform refinement of $\mathcal{T}_\ell$, i.e. all edges $E \in \mathcal{E}_\ell^\Omega \cup \mathcal{E}_\ell^\Gamma$ are halved. Let $\widehat{\mathbf{U}}_\ell \in \widehat{\mathcal{X}}_\ell$ be the Galerkin solution (13) with respect to $\widehat{\mathcal{T}}_\ell$, i.e.

$$\widehat{\mathcal{X}}_\ell := \mathcal{S}^1(\widehat{\mathcal{T}}_\ell) \times \mathcal{P}^0(\widehat{\mathcal{E}}_\ell^\Gamma),$$

where $\widehat{\mathcal{E}}_\ell^\Gamma := \widehat{\mathcal{T}}_\ell|_\Gamma$ denotes the induced boundary partition. We define the computable quantity

$$\eta_\ell := |||\widehat{\mathbf{U}}_\ell - \mathbf{U}_\ell|||. \tag{28}$$

Since the analysis of [5] is only based on the quasi-optimality estimate (11) as well as on approximation results and inverse estimates, the results directly carry over to the Johnson–Nédélec FEM–BEM coupling. The following theorem recalls some results from [5].

Theorem 6. *Let $\mathbf{u},\mathbf{u}_\ell \in \mathcal{H}$ be the exact solutions of (2) and (18), respectively. Let $\mathbf{U}_\ell \in \mathcal{X}_\ell$ and $\widehat{\mathbf{U}}_\ell \in \widehat{\mathcal{X}}_\ell$ be the Galerkin solution of (13), whereas $\mathbf{U}_\ell^\star \in \mathcal{X}_\ell$ and $\widehat{\mathbf{U}}_\ell^\star \in \widehat{\mathcal{X}}_\ell$ denote the non-perturbed Galerkin solutions (8). Then, the $(h-h/2)$-error estimator η_ℓ satisfies*

$$\eta_\ell \le C_9 |||\mathbf{u}_\ell - \mathbf{U}_\ell|||. \tag{29}$$

In particular, η_ℓ is always efficient in the sense that

$$C_{10}^{-1}\eta_\ell \le |||\mathbf{u}-\mathbf{U}_\ell||| + \mathrm{osc}_{\Gamma,\ell}. \tag{30}$$

Under the saturation assumption

$$|||\mathbf{u}-\widehat{\mathbf{U}}_\ell^\star||| \le C_{\mathrm{sat}}|||\mathbf{u}-\mathbf{U}_\ell^\star|||$$
$$\text{with some } \ell\text{-independent constant } 0 < C_{\mathrm{sat}} < 1 \tag{31}$$

for the non-perturbed problem, there holds reliability

$$C_{11}^{-1}|||\mathbf{u}-\mathbf{U}_\ell||| \le \eta_\ell + \mathrm{osc}_{\Gamma,\ell}. \tag{32}$$

Finally, the $(h-h/2)$-type error estimator

$$\mu_\ell^2 := \|\nabla(\widehat{U}_\ell - I_\ell \widehat{U}_\ell)\|_{L^2(\Omega)}^2 + \|h_\ell^{1/2}(\widehat{\Phi}_\ell - \Pi_\ell \widehat{\Phi}_\ell)\|_{L^2(\Gamma)}^2 \tag{33}$$

with $I_\ell : C(\overline{\Omega}) \to \mathcal{S}^1(\mathcal{T}_\ell)$ the nodal interpolation operator and $\Pi_\ell : L^2(\Gamma) \to \mathcal{P}^0(\mathcal{E}_\ell^\Gamma)$ the L^2-projection, is equivalent to η_ℓ, i.e.

$$C_{12}^{-1}\eta_\ell \le \mu_\ell \le C_{13}\eta_\ell. \tag{34}$$

The constant $C_9 > 0$ depends only on Ω. The constants $C_{10}, C_{12}, C_{13} > 0$ depend only on Ω and $\sigma(\mathcal{T}_0)$, whereas $C_{11} > 0$ additionally depends on the saturation constant C_{sat}. □

We remark that the saturation assumption (31) dates back to the early work [7], but may fail to hold in general [10,26]. However, it essentially states that the numerical scheme has reached an asymptotic phase [32]. For lowest-order FEM, it can be proven, if the given data are sufficiently resolved, see [26]. We stress that the saturation assumption (31) is usually observed in numerical experiments [5,32], but still remains mathematically open in the context of BEM and the FEM–BEM coupling.

Whereas the $(h-h/2)$-error estimator η_ℓ involves the non-local norm $\|\cdot\|_{\mathfrak{B}} \simeq \|\cdot\|_{H^{-1/2}(\Gamma)}$, the error estimator μ_ℓ is the sum of (weighted) local L^2-norms and can thus easily be used to steer an adaptive mesh-refinement. Moreover, since a numerical implementation will always return the improved Galerkin solution $\widehat{\mathbf{U}}_\ell$ instead of $\mathbf{U}_\ell$, it is another advantage of μ_ℓ that the computation of $\mathbf{U}_\ell$ is not needed. Finally, we stress that the Galerkin approximations $\mathbf{U}_\ell^\star$ and $\widehat{\mathbf{U}}_\ell^\star$ are only used for theoretical reasons in Theorem 6 to formulate the saturation assumption (31).

Corollary 7. *With the error estimator μ_ℓ from Theorem6 and the data oscillations from Proposition2, it holds*

$$\overline{\mu}_\ell := (\mu_\ell^2 + \mathrm{osc}_{\Gamma,\ell}^2)^{1/2} \le C_{14}|||\mathbf{u}-\mathbf{U}_\ell||| + \mathrm{osc}_{\Gamma,\ell}. \tag{35}$$

Under the saturation assumption (31), it holds

$$|||\mathbf{u}-\mathbf{U}_\ell||| \le C_{15}\overline{\mu}_\ell. \tag{36}$$

The constant $C_{14} > 0$ depends only on Ω and $\sigma(\mathcal{T}_0)$, whereas $C_{15} > 0$ additionally depends on the saturation constant C_{sat}. □

3.6. Two-level error estimator

To abbreviate notation, let $X_\ell = \mathcal{S}^1(\mathcal{T}_\ell)$ and $\widehat{X}_\ell = \mathcal{S}^1(\widehat{\mathcal{T}}_\ell)$ as well as $Y_\ell = \mathcal{P}^0(\mathcal{E}_\ell^\Gamma)$ and $\widehat{Y}_\ell = \mathcal{P}^0(\widehat{\mathcal{E}}_\ell^\Gamma)$. Let $\mathcal{K}_\ell$ and $\widehat{\mathcal{K}}_\ell$ denote the set of nodes for $\mathcal{T}_\ell$ and $\widehat{\mathcal{T}}_\ell$, respectively.

By definition of $\widehat{\mathcal{T}}_\ell$, each node $z \in \widehat{\mathcal{K}}_\ell \backslash \mathcal{K}_\ell$ is the midpoint of an edge $E \in \mathcal{E}_\ell^\Omega \cup \mathcal{E}_\ell^\Gamma$, where $\mathcal{E}_\ell^\Omega$ again denotes the set of all interior edges of the triangulation $\mathcal{T}_\ell$. For $E \in \mathcal{E}_\ell^\Omega \cup \mathcal{E}_\ell^\Gamma$, let $\zeta_E \in \widehat{X}_\ell \backslash X_\ell$ denote the fine-mesh hat function associated with the midpoint z of E. Let

- $\mathbb{P}_\ell^\Omega : H^1(\Omega) \to X_\ell$
- $\mathbb{P}_{\ell,E}^\Omega : H^1(\Omega) \to \mathrm{span}\{\zeta_E\}$

denote the H^1-orthogonal projections onto these discrete spaces. The following result is a consequence of [50, Theorem 4.1] and explicitly stated in [42, Lemma 3.1].

Lemma 8. *For each function $\widehat{V}_\ell \in \widehat{X}_\ell$, it holds*

$$C_{16}^{-1}\|\widehat{V}_\ell\|_{H^1(\Omega)}^2 \le \|\mathbb{P}_\ell^\Omega \widehat{V}_\ell\|_{H^1(\Omega)}^2 + \sum_{E \in \mathcal{E}_\ell^\Omega \cup \mathcal{E}_\ell^\Gamma} \|\mathbb{P}_{\ell,E}^\Omega \widehat{V}_\ell\|_{H^1(\Omega)}^2 \le C_{17}\|\widehat{V}_\ell\|_{H^1(\Omega)}^2, \tag{37}$$

where the constants $C_{16}, C_{17} > 0$ depend only on $\mathrm{diam}(\Omega)$ and $\sigma(\mathcal{T}_0)$. □

For each boundary edge $E \in \mathcal{E}_\ell^\Gamma$, let $\varphi_E \in \widehat{Y}_\ell \backslash Y_\ell$ denote a two-level basis function with $\mathrm{supp}(\varphi_E) = E$ and L^2-orthogonality $\langle \varphi_E, \chi_E \rangle_\Gamma = 0$, where χ_E denotes the characteristic function on E, i.e. the Haar function φ_E with value ± 1 on the first resp. second half of E. Let

- $\mathbb{P}_\ell^\Gamma : H^{-1/2}(\Gamma) \to Y_\ell$
- $\mathbb{P}_{\ell,E}^\Gamma : H^{-1/2}(\Gamma) \to \mathrm{span}\{\varphi_E\}$

denote the orthogonal projections with respect to the $\langle \cdot, \cdot \rangle_{\mathfrak{B}}$-scalar product. Then, there holds the following norm equivalence, see e.g. [27, Proposition 4.5].

Lemma 9. *For discrete functions $\widehat{\Psi}_\ell \in \widehat{Y}_\ell$, it holds*

$$C_{18}^{-1}\|\widehat{\Psi}_\ell\|_{\mathfrak{B}}^2 \le \|\mathbb{P}_\ell^\Gamma \widehat{\Psi}_\ell\|_{\mathfrak{B}}^2 + \sum_{E \in \mathcal{E}_\ell^\Gamma} \|\mathbb{P}_{\ell,E}^\Gamma \widehat{\Psi}_\ell\|_{\mathfrak{B}}^2 \le C_{19} V2 \|\widehat{\Psi}_\ell\|_{\mathfrak{B}}^2, \tag{38}$$

where the constants $C_{18}, C_{19} > 0$ depend only on Γ and the K-mesh constant $\kappa(\mathcal{E}_0)$. □

Following [42] and with the help of the aforegoing two lemmata, we now introduce the two-level error estimator τ_ℓ.

Theorem 10. *For each interior edge $E \in \mathcal{E}_\ell^\Omega$, we define the refinement indicators*

$$\tau_\ell(E) := \frac{|\langle f, \zeta_E \rangle_\Omega - \langle \nabla U_\ell, \nabla \zeta_E \rangle_\Omega|}{\|\zeta_E\|_{H^1(\Omega)}}, \tag{39}$$

whereas, for boundary edges $E \in \mathcal{E}_\ell^\Gamma$, we define

$$\tau_\ell(E) := \frac{|\langle f, \zeta_E \rangle_\Omega - \langle \nabla U_\ell, \nabla \zeta_E \rangle_\Omega + \langle \phi_0 + \Phi_\ell, \zeta_E \rangle_\Gamma|}{\|\zeta_E\|_{H^1(\Omega)}}$$
$$+ \frac{|\langle \varphi_E, (\mathfrak{K} - \frac{1}{2})(U_\ell - U_{0,\ell}) - \mathfrak{V}\Phi_\ell \rangle_\Gamma|}{\|\varphi_E\|_{\mathfrak{B}}}. \tag{40}$$

Then, the two-level error estimator

$$\tau_\ell := \left(\sum_{E\in\mathcal{E}_\ell^\Omega\cup\mathcal{E}_\ell^\Gamma}\tau_\ell(E)^2\right)^{1/2} \tag{41}$$

is equivalent to the $(h-h/2)$-error estimator η_ℓ, i.e. there holds

$$C_{20}^{-1}\eta_\ell \le \tau_\ell \le C_{21}\eta_\ell. \tag{42}$$

The constants $C_{20},C_{21}>0$ depend only on Ω and $\sigma(\mathcal{T}_0)$.

Proof. We define the scalar product

$$\langle\!\langle \mathbf{u},\mathbf{v}\rangle\!\rangle := \int_\Omega \nabla u\cdot\nabla v\,dx+\int_\Omega uv\,dx+\langle\phi,\mathfrak{V}\psi\rangle \quad \text{for all } \mathbf{u}=(u,\phi),\ \mathbf{v}=(v,\psi)\in\mathcal{H}$$

and note that $\langle\!\langle\cdot,\cdot\rangle\!\rangle$ induces the norm $|||\cdot|||$ on $\mathcal{H}$, i.e. $|||\mathbf{v}|||^2=\langle\!\langle\mathbf{v},\mathbf{v}\rangle\!\rangle$ for all $\mathbf{v}\in\mathcal{H}$. The Riesz theorem, applied to $\widehat{\mathcal{X}}_\ell$, guarantees the existence of a unique $\widehat{\mathbf{E}}_\ell=(\widehat{E}_\ell,\widehat{\varepsilon}_\ell)\in\widehat{\mathcal{X}}_\ell$ with

$$\langle\!\langle\widehat{\mathbf{E}}_\ell,\widehat{\mathbf{V}}_\ell\rangle\!\rangle = F_\ell(\widehat{\mathbf{V}}_\ell)-\mathbb{H}\mathbf{U}_\ell(\widehat{\mathbf{V}}_\ell) \quad \text{for all } \widehat{\mathbf{V}}_\ell\in\widehat{\mathcal{X}}_\ell, \tag{43}$$

where $F_\ell\in\mathcal{H}^*$ is defined in (22). Recall that (13) is equivalently stated by

$$\mathbb{H}\mathbf{U}_\ell(\mathbf{V}_\ell)=F_\ell(\mathbf{V}_\ell) \quad \text{for all } \mathbf{V}_\ell\in\mathcal{X}_\ell. \tag{44}$$

Moreover, there holds

$$|||\widehat{\mathbf{E}}_\ell||| = \|F_\ell-\mathbb{H}\mathbf{U}_\ell\|_{\widehat{\mathcal{X}}_\ell^*} = \|\mathbb{H}(\widehat{\mathbf{U}}_\ell-\mathbf{U}_\ell)\|_{\widehat{\mathcal{X}}_\ell^*} \simeq |||\widehat{\mathbf{U}}_\ell-\mathbf{U}_\ell|||,$$

where we have used that $\mathbb{H}:\widehat{\mathcal{X}}_\ell\to\widehat{\mathcal{X}}_\ell^*$ is an isomorphism as well as that $\mathbb{H}\widehat{\mathbf{U}}_\ell(\widehat{\mathbf{V}}_\ell)=F_\ell(\widehat{\mathbf{V}}_\ell)$ for all $\widehat{\mathbf{V}}_\ell\in\widehat{\mathcal{X}}_\ell$ is equivalent to $\mathbb{H}\widehat{\mathbf{U}}_\ell=F_\ell$ in $\widehat{\mathcal{X}}_\ell^*$. Let $\mathbb{P}_\ell:\mathcal{H}\to\mathcal{X}_\ell$ denote the orthogonal projection in $\mathcal{H}$, where orthogonality is understood with respect to the scalar product $\langle\!\langle\cdot,\cdot\rangle\!\rangle$. According to the symmetry of $\mathbb{P}_\ell$, definition (43) and (44) we observe

$$\begin{aligned}|||\mathbb{P}_\ell\widehat{\mathbf{E}}_\ell|||^2 &= \langle\!\langle\mathbb{P}_\ell\widehat{\mathbf{E}}_\ell,\mathbb{P}_\ell\widehat{\mathbf{E}}_\ell\rangle\!\rangle = \langle\!\langle\widehat{\mathbf{E}}_\ell,\mathbb{P}_\ell\widehat{\mathbf{E}}_\ell\rangle\!\rangle\\ &= F_\ell(\mathbb{P}_\ell\widehat{\mathbf{E}}_\ell)-\mathbb{H}\mathbf{U}_\ell(\mathbb{P}_\ell\widehat{\mathbf{E}}_\ell)=0.\end{aligned}$$

Since $\mathbb{P}_\ell=(\mathbb{P}_\ell^\Omega,\mathbb{P}_\ell^\Gamma)$, we may apply Lemmas 8 and 9 to see

$$|||\widehat{\mathbf{U}}_\ell-\mathbf{U}_\ell|||^2 \simeq \sum_{E\in\mathcal{E}_\ell^\Omega}\|\mathbb{P}_{\ell,E}^\Omega\widehat{E}_\ell\|_{H^1(\Omega)}^2+\sum_{E\in\mathcal{E}_\ell^\Gamma}(\|\mathbb{P}_{\ell,E}^\Gamma\widehat{\varepsilon}_\ell\|_{\mathfrak{V}}^2+\|\mathbb{P}_{\ell,E}^\Omega\widehat{E}_\ell\|_{H^1(\Omega)}^2). \tag{45}$$

The right-hand side is, in fact, the two-level error estimator τ_ℓ defined in (39) and (40). Therefore, (45) proves that the two-level error estimator τ_ℓ is equivalent to the $(h-h/2)$-error estimator $\eta_\ell=|||\widehat{\mathbf{U}}_\ell-\mathbf{U}_\ell|||$ from Theorem 6, where the equivalence constants depend only on Ω and $\sigma(\mathcal{T}_0)$. This concludes the proof. □

Corollary 11. *With the two-level error estimator τ_ℓ from Theorem 10 and the data oscillations from Proposition2, it holds*

$$\overline{\tau}_\ell := (\tau_\ell^2+\mathrm{osc}_{\Gamma,\ell}^2)^{1/2} \le C_{22}(|||\mathbf{u}-\mathbf{U}_\ell|||+\mathrm{osc}_{\Gamma,\ell}). \tag{46}$$

Under the saturation assumption (31), *it holds*

$$|||\mathbf{u}-\mathbf{U}_\ell||| \le C_{23}\overline{\tau}_\ell. \tag{47}$$

The constant $C_{22}>0$ depends only on Ω and $\sigma(\mathcal{T}_0)$, whereas $C_{23}>0$ additionally depends on the saturation constant C_{sat}.

Proof. The proof follows from $\overline{\tau}_\ell\simeq\eta_\ell+\mathrm{osc}_{\Gamma,\ell}$ and estimates (30)–(32) from Theorem 6. □

3.7. Local estimates for residual and two-level indicators

According to Theorems 4, 6, and 10, it holds that

$$\tau_\ell\simeq\eta_\ell\lesssim|||\mathbf{u}_\ell-\mathbf{U}_\ell|||\lesssim\varrho_\ell.$$

In this section, we prove that the estimate $\tau_\ell\lesssim\varrho_\ell$ holds even locally. To that end, we write the residual error estimator ϱ_ℓ from (21) as sum

$$\varrho_\ell^2=\sum_{E\in\mathcal{E}_\ell^\Omega}\varrho_\ell(E)^2+\sum_{E\in\mathcal{E}_\ell^\Gamma}\varrho_\ell(E)^2 \tag{48}$$

of certain local contributions. For an interior edge $E\in\mathcal{E}_\ell^\Omega$, we define

$$\varrho_\ell(E)^2 := \gamma_\ell(E)^2+\mathrm{osc}_{\Omega,\ell}(E)^2, \tag{49}$$

whereas for a boundary edge $E\in\mathcal{E}_\ell^\Gamma$, there holds

$$\begin{aligned}&\varrho_\ell(E)^2:\\ &\quad=\|h_\ell^{1/2}(\phi_0+\Phi_\ell-\partial_nU_\ell)\|_{L^2(E)}^2+\|h_\ell^{1/2}((\tfrac12-\mathfrak{K})(U_{0,\ell}-U_\ell)-\mathfrak{V}\Phi_\ell)'\|_{L^2(E)}^2.\end{aligned} \tag{50}$$

Comparing these with the local contributions $\tau_\ell(E)$ from (39)–(40), we obtain the following result.

Theorem 12. *For each interior edge $E\in\mathcal{E}_\ell^\Omega$, it holds*

$$C_{24}^{-1}\tau_\ell(E)\le\varrho_\ell(\mathcal{E}_{\ell,z}) \quad \text{for all } z\in(E\cap\mathcal{K}_\ell)\backslash\Gamma. \tag{51}$$

For each boundary edge $E\in\mathcal{E}_\ell^\Gamma$ and the unique element $T\in\mathcal{T}_\ell$ with $E=\partial T\cap\Gamma$, it holds

$$C_{25}^{-1}\tau_\ell(E)\le\varrho_\ell(E)+\varrho_\ell(\mathcal{E}_{\ell,z}) \quad \text{with } z=(T\cap\mathcal{K}_\ell)\backslash\Gamma. \tag{52}$$

The constants $C_{24},C_{25}>0$ depend only on Ω and $\sigma(\mathcal{T}_0)$.

Proof. According to uniform shape regularity, we first note that

$$\|\zeta_E\|_{L^2(\Omega)}\simeq\mathrm{diam}(T),\quad \|\zeta_E\|_{L^2(E)}\simeq\mathrm{diam}(E)^{1/2},\quad \|\nabla\zeta_E\|_{L^2(\Omega)}\simeq1,$$

where $T\in\mathcal{T}_\ell$ is an arbitrary element with $E\subset\partial T$. The constants in the latter estimates depend only on an upper bound of $\sigma(\mathcal{T}_\ell)$.

For an interior edge $E=T_+\cap T_-\in\mathcal{E}_\ell^\Omega$, piecewise integration by parts shows

$$\begin{aligned}\tau_\ell(E)&\le\frac{\|f\|_{L^2(T_+\cup T_-)}\|\zeta_E\|_{L^2(T_+\cup T_-)}+\|[\partial_nU_\ell]\|_{L^2(E)}\|\zeta_E\|_{L^2(E)}}{\|\nabla\zeta_E\|_{L^2(\Omega)}}\\ &\lesssim\|h_\ell f\|_{L^2(T_+\cup T_-)}+\gamma_\ell(E).\end{aligned} \tag{53}$$

For each node $z\in(E\cap\mathcal{K}_\ell)\backslash\Gamma$, Lemma 3 yields $\|h_\ell f\|_{L^2(T_+\cup T_-)}\lesssim\gamma_\ell(\mathcal{E}_{\ell,z})+\mathrm{osc}_{\Omega,\ell}(\mathcal{E}_{\ell,z})=\varrho_\ell(\mathcal{E}_{\ell,z})$. This and $\gamma_\ell(E)\le\varrho_\ell(E)\lesssim\varrho_\ell(\mathcal{E}_{\ell,z})$ conclude (51).

For a boundary edge $E=T\cap\Gamma\in\mathcal{E}_\ell^\Gamma$, we use integration by parts and norm equivalence $\|\varphi_E\|_{H^{-1/2}(\Gamma)}\simeq\|\varphi_E\|_{\mathfrak{V}}$ to estimate

$$\begin{aligned}\tau_\ell(E)&\le\frac{\|f\|_{L^2(T)}\|\zeta_E\|_{L^2(T)}+\|\phi_0+\Phi_\ell-\partial_nU_\ell\|_{L^2(E)}\|\zeta_E\|_{L^2(E)}}{\|\nabla\zeta_E\|_{L^2(T)}}\\ &\quad+\|\left(\frac12-\mathfrak{K}\right)(U_{0,\ell}-U_\ell)-\mathfrak{V}\Phi_\ell\|_{L^2(E)}\frac{\|\varphi_E\|_{L^2(E)}}{\|\varphi_E\|_{\mathfrak{V}}}\\ &\lesssim\|h_\ell f\|_{L^2(T)}+\|h_\ell^{1/2}(\phi_0+\Phi_\ell-\partial_nU_\ell)\|_{L^2(E)}\\ &\quad+\left\|h_\ell^{-1/2}\left(\left(\frac12-\mathfrak{K}\right)(U_{0,\ell}-U_\ell)-\mathfrak{V}\Phi_\ell\right)\right\|_{L^2(E)},\end{aligned} \tag{54}$$

where we used an inverse estimate $\|h_\ell^{1/2}\varphi_E\|_{L^2(\Gamma)}\lesssim\|\varphi_E\|_{H^{-1/2}(\Gamma)}$ for $\varphi_E\in\widehat{Y}_\ell\backslash Y_\ell$. By use of the second equation in (13), we obtain

$$\int_E w\,d\Gamma=\langle\chi_E,w\rangle_\Gamma=0 \quad \text{for } w:=(\tfrac12-\mathfrak{K})(U_{0,\ell}-U_\ell)-\mathfrak{V}\Phi_\ell\in H^1(\Gamma).$$

Therefore, we may apply the Poincaré inequality on E to see

$$\begin{aligned}&\left\|h_\ell^{-1/2}\left(\left(\frac12-\mathfrak{K}\right)(U_{0,\ell}-U_\ell)-\mathfrak{V}\Phi_\ell\right)\right\|_{L^2(E)}\\ &\quad\le\frac{1}{\pi}\left\|h_\ell^{1/2}\left(\left(\frac12-\mathfrak{K}\right)(U_{0,\ell}-U_\ell)-\mathfrak{V}\Phi_\ell\right)'\right\|_{L^2(E)}.\end{aligned} \tag{55}$$

The combination of (54)–(55) thus proves

$$\tau_\ell(E)\lesssim\|h_\ell f\|_{L^2(T)}+\varrho_\ell(E).$$

Finally, Lemma 3 gives $\|h_\ell f\|_{L^2(T)} \lesssim \varrho_\ell(\mathcal{E}_{\ell,z})$ with $z=(T\cap\mathcal{K}_\ell)\backslash T$ the interior node of T. □

To state the final theorem, let Π_ℓ denote the L^2-orthogonal projections $\Pi_\ell : L^2(\Gamma)\to\mathcal{P}^0(\mathcal{E}_\ell^\Gamma)$ and $\Pi_\ell : L^2(\Omega)\to\mathcal{P}^0(\mathcal{T}_\ell)$, respectively. Furthermore, we define the mesh quantities

$$h_{\ell,\max} := \max\{\operatorname{diam}(E) : E\in\mathcal{E}_\ell^\Gamma\}$$

and

$$h_{\ell,\min} := \min\{\operatorname{diam}(E) : E\in\mathcal{E}_\ell^\Gamma\}.$$

With these ingredients, we have the following efficiency-type estimate in case that the boundary partition $\mathcal{E}_\ell^\Gamma$ is quasi-uniform. The proof follows by adaption of the arguments of [11] to the Johnson–Nédélec coupling. Since the details are, however, quite lengthy and technical and since the result is comparably weak (cf. the discussion in Section 5), we refer to the preprint [4].

Theorem 13. *We assume that the exact solution* $\mathbf{u}=(u,\phi)$ *of* (2) *satisfies the additional regularity assumption* $u|_\Gamma\in H^1(\Gamma)$ *and* $\phi\in L^2(\Gamma)$. *Then, it holds that*

$$C_{26}^{-1}\varrho_\ell \le \frac{h_{\ell,\max}^{1/2}}{h_{\ell,\min}^{1/2}}|||\mathbf{u}-\mathbf{U}_\ell||| + \frac{h_{\ell,\max}}{h_{\ell,\min}^{1/2}}(\|\phi-\Pi_\ell\phi\|_{L^2(\Gamma)}+\|u-I_\ell u\|_{H^1(\Gamma)}) + \|h_\ell(f-\Pi_\ell f)\|_{L^2(\Omega)} + \|h_\ell^{1/2}(\phi_0-\Pi_\ell\phi_0)\|_{L^2(\Gamma)} + h_{\ell,\max}^{1/2}\|(u_0-U_{0,\ell})'\|_{L^2(\Gamma)},$$

where the constant $C_{26}>0$ *depends only on* Ω, *the shape regularity constant* $\sigma(\mathcal{T}_\ell)$, *and the K mesh constant* $\kappa(\mathcal{E}_\ell^\Gamma)$. □

4. Numerical experiments

In this section, we present a numerical example to compare the different error estimators and demonstrate the advantages of adaptive mesh refinement compared with uniform refinement. At first, we consider the error estimator v_ℓ which is a placeholder for the presented estimators ϱ_ℓ, μ_ℓ, or τ_ℓ. The adaptive algorithms (cf. Algorithm 14–16) use Dörfler marking [25] with an adaptivity parameter $\theta\in(0,1)$, i.e.

$$\theta\overline{v}_\ell^2 := \theta(v_\ell^2+\operatorname{osc}_{\Gamma,\ell}^2) \le \sum_{\tau\in\mathcal{M}_\ell} v_\ell(\tau)^2 + \sum_{E\in\mathcal{M}_\ell\cap\mathcal{E}_\ell^\Gamma}\operatorname{osc}_{\Gamma,\ell}(E)^2, \tag{56}$$

where $\mathcal{M}_\ell\subseteq\mathcal{T}_\ell\cup\mathcal{E}_\ell^\Omega\cup\mathcal{E}_\ell^\Gamma$ is the set of marked elements and the local contributions $v_\ell(\tau)$ are defined in the respective Sections 4.2–4.4. The local data oscillations are defined by

$$\operatorname{osc}_{\Gamma,\ell}(E) := \|h_\ell^{1/2}(u_0-U_{0,\ell})'\|_{L^2(E)} \quad \text{for all } E\in\mathcal{E}_\ell^\Gamma. \tag{57}$$

We prescribe the exact solution $(u^{\mathrm{int}},u^{\mathrm{ext}})$ of the transmission problem (1), and the data (u_0,ϕ_0,f) are computed from there. Note that the contribution $\|\phi-\Phi_\ell\|_{\mathfrak{B}}$ to the error $|||\mathbf{u}-\mathbf{U}_\ell|||$ can hardly be computed analytically. However, with the quasi-optimality (11) it holds that

$$|||\mathbf{u}-\mathbf{U}_\ell||| \lesssim |||\mathbf{u}-\mathbf{U}_\ell^\star||| + \operatorname{osc}_{\Gamma,\ell} \lesssim \|u-U_\ell\|_{H^1(\Omega)} + \min_{\Psi_\ell\in\mathcal{P}^0(\mathcal{E}_\ell^\Gamma)}\|\phi-\Psi_\ell\|_{\mathfrak{B}} + \operatorname{osc}_{\Gamma,\ell}$$

with $\mathbf{u}=(u,\phi)$ and $\mathbf{U}_\ell=(U_\ell,\Phi_\ell)$. In our experiment, the exterior normal derivative has additional regularity $\phi\in L^2(\Gamma)$. We therefore obtain

$$\min_{\Psi_\ell\in\mathcal{P}^0(\mathcal{E}_\ell^\Gamma)}\|\phi-\Psi_\ell\|_{\mathfrak{B}} \le \|(1-\Pi_\ell)\phi\|_{\mathfrak{B}} \lesssim \|h_\ell^{1/2}(1-\Pi_\ell)\phi\|_{L^2(\Gamma)} \le \|h_\ell^{1/2}(\phi-\Phi_\ell)\|_{L^2(\Gamma)}$$

with $\Pi_\ell : L^2(\Gamma)\to\mathcal{P}^0(\mathcal{T}_\ell)$ being the L^2-orthogonal projection, see [15, Theorem 4.1]. Altogether, we see that

$$|||\mathbf{u}-\mathbf{U}_\ell||| \lesssim \|u-U_\ell\|_{H^1(\Omega)} + \|h_\ell^{1/2}(\phi-\Phi_\ell)\|_{L^2(\Gamma)} + \operatorname{osc}_{\Gamma,\ell} =: \operatorname{err}_\ell(u)+\operatorname{err}_\ell(\phi)+\operatorname{osc}_{\Gamma,\ell} =: \operatorname{err}_\ell \tag{58}$$

provides a computable upper bound for the energy error. In the same spirit, the error estimator v_ℓ is split into

$$v_\ell^2 = \sum_{\tau\in\mathcal{T}_\ell\cup\mathcal{E}_\ell^\Omega} v_\ell(\tau)^2 + \sum_{E\in\mathcal{E}_\ell^\Gamma} v_\ell(E)^2 =: v_\ell(u)^2+v_\ell(\phi)^2. \tag{59}$$

Empirically, we have evidence that for all three estimators it holds

$$\overline{v}_\ell := v_\ell(u)+v_\ell(\phi)+\operatorname{osc}_{\Gamma,\ell} \lesssim |||\mathbf{u}-\mathbf{U}_\ell||| + \operatorname{osc}_{\Gamma,\ell} \lesssim v_\ell(u)+v_\ell(\phi)+\operatorname{osc}_{\Gamma,\ell} = \overline{v}_\ell, \tag{60}$$

where we can prove the lower bound for μ_ℓ and τ_ℓ (Theorems 6 and 11). However, for ϱ_ℓ the lower bound is only proven on quasi-uniform meshes (Theorem 13). The upper bound holds for ϱ_ℓ without restrictions (Theorem 5) whereas it holds for μ_ℓ and ϱ_ℓ only under the saturation assumption (Theorem 6 and 11).

In the following, we plot the five quantities $\operatorname{err}_\ell(u)$, $\operatorname{err}_\ell(\phi)$, $v_\ell(u)$, $v_\ell(\phi)$, and $\operatorname{osc}_{\Gamma,\ell}$ from (58)–(59) over the number $N=\mathcal{T}_\ell$ of triangles, where both axes are scaled logarithmically. We consider uniform mesh-refinement $\mathcal{T}_\ell=\mathcal{T}_\ell^{(\mathrm{unif})}$ with $\mathcal{T}_\ell^{(\mathrm{unif})} := \widehat{\mathcal{T}}_{\ell-1}$, cf. Section 3.2, as well as adaptive mesh-refinement, where the sequence of meshes $\mathcal{T}_\ell=\mathcal{T}_\ell^{(\mathrm{adap})}$ is generated by the Algorithms 14–16 with $\theta=0.25$. Note that a decay with slope $-\alpha$ indicates some dependence $\mathcal{O}(N^{-\alpha})$. For uniform meshes with mesh-size h, this corresponds to $\mathcal{O}(h^{2\alpha})$. We stress that, by theory, an overall slope of $\alpha=1/2$ is thus optimal with P1-finite elements.

For the adaptive mesh-refinement of Algorithms 15 and 16, recall that all integral operators have to be computed with respect to the fine mesh $\widehat{\mathcal{T}}_\ell$. Consequently, we then consider $\widehat{\operatorname{osc}}_{\Gamma,\ell}=\|h_\ell^{1/2}(u_0-\widehat{U}_{0,\ell})'\|_{L^2(\Gamma)}$ instead of $\operatorname{osc}_{\Gamma,\ell}$. We stress that all results of this paper hold with $\operatorname{osc}_{\Gamma,\ell}$ replaced by $\widehat{\operatorname{osc}}_{\Gamma,\ell}$ as well. Moreover, although $\mathbf{U}_\ell$ is not needed by Algorithm 15, we nevertheless plot err_ℓ to give a fair comparison of uniform and adaptive mesh-refinement.

Besides the experimental convergence rates, we plot $\operatorname{err}_\ell(u)$, $\operatorname{err}_\ell(\phi)$, $v_\ell(u)$, $v_\ell(\phi)$, and $\operatorname{osc}_{\Gamma,\ell}$ (resp. $\widehat{\operatorname{osc}}_{\Gamma,\ell}$) over the computational time t_ℓ.

- For uniform mesh-refinement, $t_\ell=t_\ell^{(\mathrm{unif})}$ is the time needed for ℓ uniform refinements of the initial mesh $\mathcal{T}_0$ to obtain $\mathcal{T}_\ell$, plus the time for building and solving the Galerkin system with respect to $\mathcal{X}_\ell$.

For adaptive mesh-refinement, $\mathcal{T}_\ell$ depends on the entire history of preceding meshes (and solutions). Therefore, the computational time has to be defined differently. Set $t_{-1}^{(\mathrm{adap})} := 0$.

- For adaptive mesh-refinement, $t_\ell=t_\ell^{(\mathrm{adap})}$ is the sum of the time $t_{\ell-1}^{(\mathrm{adap})}$ elapsed in prior steps of the adaptive algorithm, plus the time for performing one adaptive step on the ℓ-th mesh, i.e. steps (i)–(vi) of Algorithms 15 and 16 or steps (i)–(v) of Algorithm 14.

Although this definition seems to favor uniform mesh-refinement, adaptive mesh-refinement will empirically turn out to be superior. All experiments are conducted by use of MATLAB (Release 2009b) running on a common 64 Bit Linux system with 32 GB of RAM. Throughout, the occurring linear systems are solved by use of the MATLAB backslash operator. For the computation of the boundary integral operators, we use the MATLAB BEM library HILBERT, cf. [2]; see http://www.asc.tuwien.ac.at/abem/hilbert/ for details.

4.1. The problem

We consider the Z-shaped domain visualized in Fig. 2. We prescribe the exact solution of (1) as

$$u^{\mathrm{int}}(x,y) = r^{4/7}\sin(\tfrac{4}{7}\varphi) \quad \text{in } \Omega^{\mathrm{int}},$$

$$u^{\mathrm{ext}}(x,y) = \frac{x+y+0.25}{(x+0.125)^2+(y+0.125)^2} \quad \text{in } \Omega^{\mathrm{ext}}, \tag{61}$$

where (r,φ) are the polar coordinates of $(x,y) \in \mathbb{R}^2$ with respect to (0,0). Recall that (u,ϕ) denotes the exact solution of (2) and note that $u = u^{\mathrm{int}}$ has a generic singularity at the reentrant corner, whereas $\phi = \nabla u^{\mathrm{ext}} \cdot n$ is piecewise smooth. Note that $-\Delta u^{\mathrm{int}} = 0 = -\Delta u^{\mathrm{ext}}$, whence $\mathrm{osc}_{\Omega,\ell} = 0$ for all $\ell \in \mathbb{N}$.

4.2. Experiment with residual-based error estimator ϱ_ℓ

For the residual-based error estimator ϱ_ℓ, we define the local contributions as follows:

$$\varrho_\ell(E)^2 := \mathrm{osc}_{\Omega,\ell}(E)^2 + \gamma_\ell(E)^2 \quad \text{for all } E \in \mathcal{E}_\ell^\Omega,$$

$$\varrho_\ell(E)^2 := \|h_\ell^{1/2}(\phi_0 + \Phi_\ell - \partial_n U_\ell)\|_{L^2(E)}^2 + \|h_\ell^{1/2}((\tfrac{1}{2}-\mathfrak{K})(U_{0,\ell}-U_\ell) - \mathfrak{V}\Phi_\ell)'\|_{L^2(E)}^2 \quad \text{for all } E \in \mathcal{E}_\ell^\Gamma. \tag{62}$$

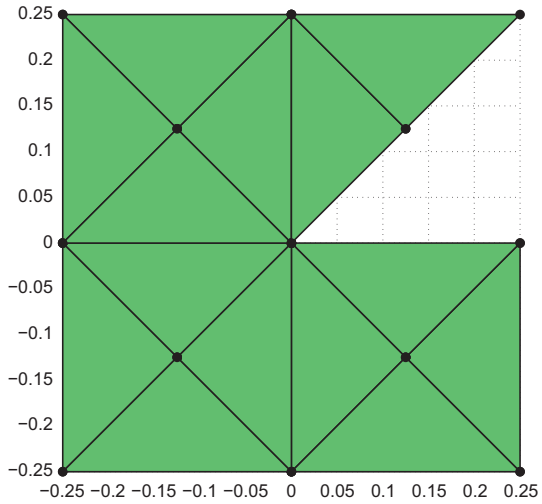

Fig. 2. Z-shaped domain and initial triangulation $\mathcal{T}_0$ for the numerical experiment.

The adaptive algorithm for the residual-based error estimator $\overline{\varrho}_\ell$ reads as follows:

Algorithm 14. Input: Initial meshes $(\mathcal{T}_0,\mathcal{E}_0)$ for $\ell := 0$, adaptivity parameter $\theta \in (0,1)$.

(i) Compute discrete solution $\mathbf{U}_\ell \in \mathcal{X}_\ell$.
(ii) Compute refinement indicators $\overline{\varrho}_\ell(\tau)$ for all $\tau \in \mathcal{E}_\ell^\Omega \cup \mathcal{E}_\ell^\Gamma$.
(iii) Determine set $\mathcal{M}_\ell \subseteq \mathcal{E}_\ell^\Omega \cup \mathcal{E}_\ell^\Gamma$ which satisfies Dörfler marking (56).
(iv) Mark edges $E \in \mathcal{E}_\ell \cap \mathcal{M}_\ell$ for refinement.
(v) Generate new meshes $(\mathcal{T}_{\ell+1},\mathcal{E}_{\ell+1}^\Gamma)$, increase counter $\ell \mapsto \ell+1$, and goto (i).

Output: Sequence of error estimators $(\overline{\varrho}_\ell)_{\ell\in\mathbb{N}}$ and discrete solutions $(\mathbf{U}_\ell)_{\ell\in\mathbb{N}}$. □

In Fig. 3, we plot the convergence of the error quantities from (58)–(59). Since the interior solution has a generic singularity at the reentrant corner, uniform mesh-refinement leads to a sub-optimal order of convergence $\alpha = 2/7$, i.e. we observe $\mathcal{O}(h^{4/7})$. For $\mathrm{err}_\ell(u)$ and $\varrho_\ell(u)$, this asymptotic is observed already on coarse meshes. For $\mathrm{err}_\ell(\phi)$ and $\varrho_\ell(\phi)$, a preasymptotic phase occurs. For adaptive mesh-refinement, we observe the optimal order of convergence $\alpha = 1/2$ for $\mathrm{err}_\ell(u)$ and $\varrho_\ell(u)$. Moreover, the terms $\mathrm{err}_\ell(\phi)$ and $\varrho_\ell(\phi)$ even converge with order $\mathcal{O}(h^{3/2})$ which is optimal for the approximation of a smooth function by piecewise constants with respect to the $H^{-1/2}(\Gamma)$-norm.

The plots of Fig. 3 provide comparisons between uniform and adaptive mesh-refinement. We plot $\overline{\varrho}$ from (60) as well as err_ℓ from (58) over the computational time. Both plots underline that the proposed adaptive algorithm is superior to uniform mesh-refinement.

4.3. Experiment with $(h-h/2)$-type error estimator μ_ℓ

With the local contributions of μ_ℓ defined by

$$\mu_\ell(T)^2 = \|(1-I_\ell)\widehat{U}_\ell\|_{H^1(T)}^2 \tag{63}$$

for triangles $T \in \mathcal{T}_\ell$ and by

$$\mu_\ell(E)^2 = \mathrm{diam}(E)\|(1-\Pi_\ell)\widehat{\Phi}_\ell\|_{L^2(E)}^2 \tag{64}$$

for line segments $E \in \mathcal{E}_\ell^\Gamma$, we consider the *convergent* adaptive algorithm proposed in [5].

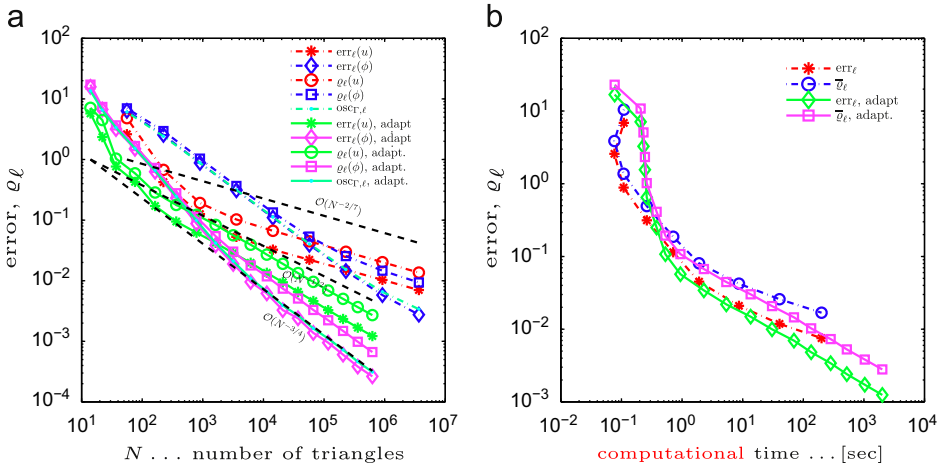

Fig. 3. Estimators $\mathrm{err}_\ell(u)$, $\mathrm{err}_\ell(\phi)$, $\varrho_\ell(u)$ and $\varrho_\ell(\phi)$ from (58)–(59) as well as data oscillations $\mathrm{osc}_{\Gamma,\ell}$ plotted over the number $N = \mathcal{T}_\ell$ of triangles (left) and over the computational time (right).

Algorithm 15. Input: Initial meshes $(\mathcal{T}_0,\mathcal{E}_0)$ for $\ell := 0$, adaptivity parameter $\theta \in (0,1)$.

(i) Generate uniformly refined meshes $\widehat{\mathcal{T}}_\ell$, $\widehat{\mathcal{E}}_\ell^\Gamma$.
(ii) Compute discrete solution $\widehat{\mathbf{U}}_\ell \in \widehat{\mathcal{X}}_\ell$.
(iii) Compute refinement indicators $\overline{\mu}_\ell(\tau)$ for all $\tau \in \mathcal{T}_\ell \cup \mathcal{E}_\ell^\Gamma$.
(iv) Determine set $\mathcal{M}_\ell \subseteq \mathcal{T}_\ell \cup \mathcal{E}_\ell^\Gamma$ which satisfies Dörfler marking (56).
(v) Mark triangles $T \in \mathcal{T}_\ell \cap \mathcal{M}_\ell$ and boundary elements $E \in \mathcal{E}_\ell^\Gamma \cap \mathcal{M}_\ell$ for refinement.
(vi) Generate new meshes $(\mathcal{T}_{\ell+1},\mathcal{E}_{\ell+1}^\Gamma)$, increase counter $\ell \mapsto \ell+1$, and goto (i).

Output: Sequence of error estimators $(\overline{\mu}_\ell)_{\ell\in\mathbb{N}}$ and discrete solutions $(\widehat{\mathbf{U}}_\ell)_{\ell\in\mathbb{N}}$. □

Fig. 4 provides the experimental convergence results for the experiment. The observations for the convergence rate are the same as in Section 4.2. The advantage in computational time takes effect after a long preasymptotic phase.

4.4. Experiment with two-level error estimator τ_ℓ

The local contributions $\tau_\ell(E)$ for $E \in \mathcal{E}_\ell^\Gamma \cup \mathcal{E}_\ell^\Omega$ are defined in Theorem 11. Similar to the $(h-h/2)$-based adaptive algorithm for $\overline{\mu}_\ell$ the algorithm for the two-level error estimator $\overline{\tau}_\ell$ reads as follows:

Algorithm 16. Input: Initial meshes $(\mathcal{T}_0,\mathcal{E}_0)$ for $\ell := 0$, adaptivity parameter $\theta \in (0,1)$.

(i) Compute discrete solution $\mathbf{U}_\ell \in \mathcal{X}_\ell$.
(ii) Generate uniformly refined meshes $\widehat{\mathcal{T}}_\ell$, $\widehat{\mathcal{E}}_\ell^\Gamma$.
(iii) Compute refinement indicators $\overline{\tau}_\ell(\tau)$ for all $\tau \in \mathcal{E}_\ell^\Omega \cup \mathcal{E}_\ell^\Gamma$.
(iv) Determine set $\mathcal{M}_\ell \subseteq \mathcal{E}_\ell^\Omega \cup \mathcal{E}_\ell^\Gamma$ which satisfies Dörfler marking (56).
(v) Mark edges $E \in \mathcal{E}_\ell \cap \mathcal{M}_\ell$ for refinement.
(vi) Generate new meshes $(\mathcal{T}_{\ell+1},\mathcal{E}_{\ell+1}^\Gamma)$, increase counter $\ell \mapsto \ell+1$, and goto (i).

Output: Sequence of error estimators $(\overline{\tau}_\ell)_{\ell\in\mathbb{N}}$ and discrete solutions $(\mathbf{U}_\ell)_{\ell\in\mathbb{N}}$. □

Fig. 5 provides the experimental convergence results.

4.5. Comparison of ϱ_ℓ, μ_ℓ, and τ_ℓ

Now, we want to compare the three proposed estimators in terms of convergence rate and time consumption. We plot the quantities

$$\mathrm{err}_\ell(v) := (\mathrm{err}_\ell(u)^2 + \mathrm{err}_\ell(\phi)^2 + \mathrm{osc}_{\Gamma,\ell}^2)^{1/2} \quad \text{as well as} \quad \overline{\nu}_\ell, \tag{65}$$

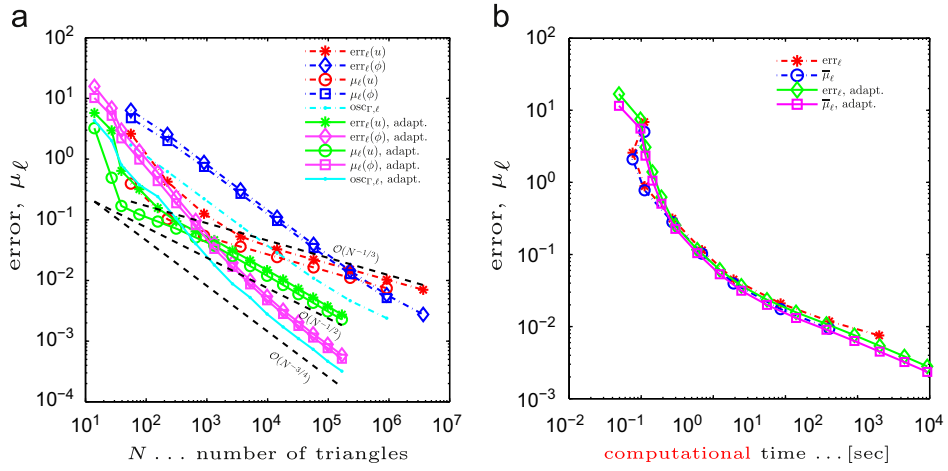

Fig. 4. Estimators $\mathrm{err}_\ell(u)$, $\mathrm{err}_\ell(\phi)$, $\mu_\ell(u)$ and $\mu_\ell(\phi)$ from (58)–(59) as well as data oscillations $\mathrm{osc}_{\Gamma,\ell}$ plotted over the number $N = \mathcal{T}_\ell$ of triangles (left) and over the computational time (right).

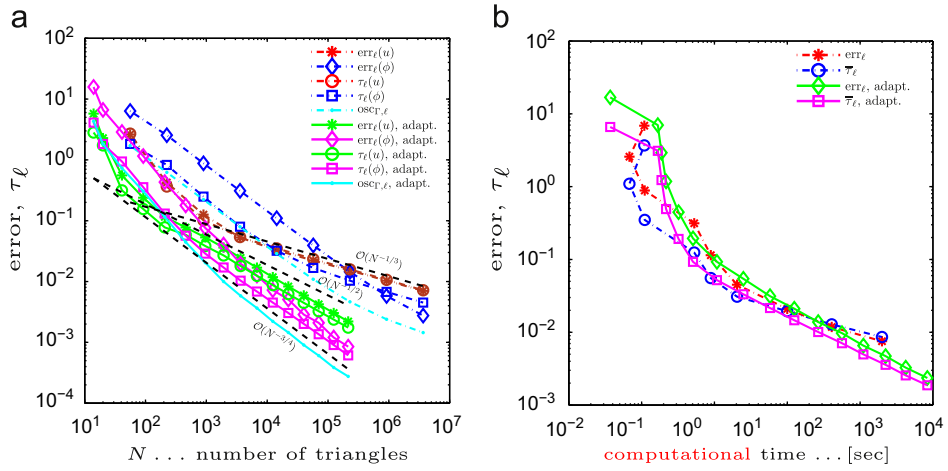

Fig. 5. Estimators $\mathrm{err}_\ell(u)$, $\mathrm{err}_\ell(\phi)$, $\tau_\ell(u)$ and $\tau_\ell(\phi)$ from (58)–(59) as well as data oscillations $\mathrm{osc}_{\Gamma,\ell}$ plotted over the number $N = \mathcal{T}_\ell$ of triangles (left) and over the computational time (right).

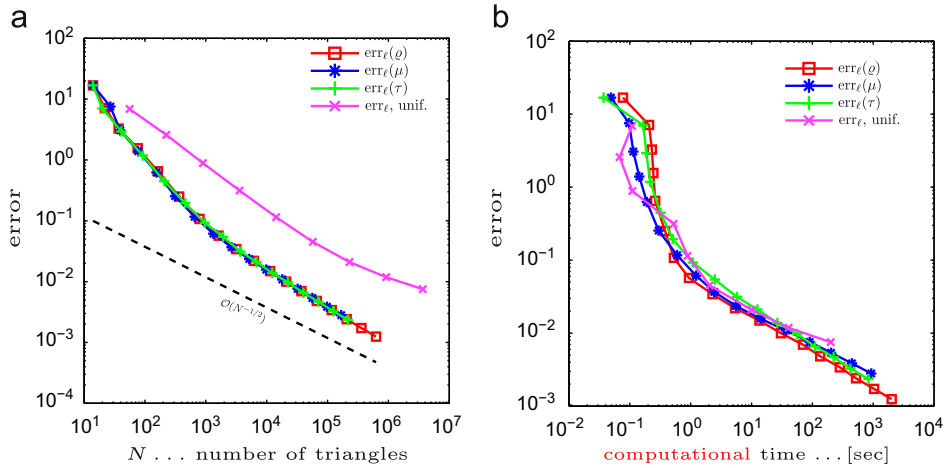

Fig. 6. Error quantities $\mathrm{err}_\ell(\varrho)$, $\mathrm{err}_\ell(\mu)$, $\mathrm{err}_\ell(\tau)$ for the three adaptive algorithms and err_ℓ for uniform mesh-refinement plotted over the number $N=\mathcal{T}_\ell$ of triangles (left) and over the computational time (right).

where the adaptive algorithm is steered by the estimator $\overline{\nu}_\ell$ from (60) and $\nu_\ell\in\{\varrho_\ell,\mu_\ell,\tau_\ell\}$. Note that all three estimators produce the same rate of convergence, but we observe significant differences in the plot on the right-hand side, cf. Fig. 6.

5. Conclusions and remarks

5.1. Analytical results

In this work, we have transferred the a posteriori error analysis for some 2D FEM–BEM model problem from the symmetric coupling [22] to the Johnson–Nédélec coupling [37]. We have analytically and numerically studied certain computable upper (*reliable*) and lower (*efficient*) bounds of the FEM–BEM error $|||\mathbf{u}-\mathbf{U}_\ell|||$ in the energy norm. Altogether, three different types of a posteriori error estimators and corresponding adaptive mesh-refinement techniques have been considered.

First, we adapted the weighted-residual approach from the seminal work [20]. Contrary to the original work, our variant of the estimator ϱ_ℓ involves edge oscillations $\mathrm{osc}_{\Omega,\ell}$ instead of the volume residuals $\|h_\ell f\|_{L^2(\Omega)}$. Thus, the interior edge jumps generically dominate the a posteriori error estimate in the sense that, in numerical experiments, adaptive mesh-refinement empirically leads to optimal convergence behavior $\varrho_\ell=\mathcal{O}(N^{-1/2})=\gamma_\ell$ for the interior jumps, whereas the other contributions even appear to be of higher order. Corollary 5 states reliability of ϱ_ℓ, i.e. up to data oscillations ϱ_ℓ provides an upper bound for the error.

Second, we observed that the $(h-h/2)$-based approach of [5] carries over to the Johnson–Nédélec formulation without any modification. In Theorem 6, we collected the results from [5] on the canonical estimator η_ℓ and its localized and simplified variant μ_ℓ. The latter might be attractive from an implementational point of view since there is almost no overhead for its realization.

Third, we proved that the two-level error estimation technique from [42] can be used for the Johnson–Nédélec formulation as well. For our linear model problem, Theorem 10 states that this estimator is equivalent to the $(h-h/2)$-estimator from [5]. As a consequence, we could relax the saturation assumption of [42] in the following sense: In [42], the authors assumed linear convergence $|||\mathbf{u}-\mathbf{U}_{\ell+1}|||\le\kappa|||\mathbf{u}-\mathbf{U}_\ell|||$ with some $0<\kappa<1$ of the adaptively generated solutions $\mathbf{U}_\ell$ and then derived reliability and efficiency of the two-level estimator τ_ℓ from that assumption. Contrary, we only assume that uniform refinement of the triangulation $\mathcal{T}_\ell$ leads to a uniform improvement of the error, see our statement of the saturation assumption in (31). Our analysis shows that only the upper bound hinges on the saturation assumption (31), whereas efficiency holds in general. Moreover, besides the global relation $\tau_\ell\lesssim\varrho_\ell$ between the two-level error estimator τ_ℓ and the residual error estimator ϱ_ℓ, we proved that this estimate holds even locally (Theorem 12). Estimates of this type have first been observed for BEM in [13].

5.2. Numerical results

In our numerical experiments, we observe throughout that the curves of the error estimators $\nu_\ell\in\{\overline{\varrho}_\ell,\overline{\mu}_\ell,\overline{\tau}_\ell\}$ and the error bound err_ℓ are parallel for uniform as well as adaptive mesh-refinement. This gives numerical evidence for the efficiency *and* reliability of all estimators. First, this confirms reliability of $\overline{\varrho}_\ell$ (Corollary 5) as well as efficiency of $\overline{\mu}_\ell$ (Corollary 7) and $\overline{\tau}_\ell$ (Corollary 11). Second, it indicates that the efficiency of the residual error estimator ϱ_ℓ holds at least under much weaker assumption than those of Theorem 13. Third, we obtain numerical evidence for the saturation assumption which guarantees the reliability of $\overline{\mu}_\ell$ as well as $\overline{\tau}_\ell$.

Moreover, we observe that the three proposed adaptive algorithms regain the optimal order of convergence $\mathcal{O}(N^{-1/2})$ with respect to the number $N=\mathcal{T}_\ell$ of elements. Contrary, uniform mesh-refinement usually suffers from singularities of the unknown solution and/or the given data and only leads to suboptimal convergence behavior. With respect to computational time, we see that already for a tolerance $|||\mathbf{u}-\mathbf{U}_\ell|||\sim10^{-1}$ adaptive mesh-refinement is superior to a uniform approach, although the time-measurement in the adaptive case includes some error estimation which we neglect in case of uniform mesh-refinement. The tolerance 10^{-1} is satisfied for about $N=10{,}000$ uniform resp. $N=700$ adaptive elements, see Fig. 6.

An overall comparison of the considered error estimators can be concluded as follows: The adaptive algorithms driven by ϱ_ℓ (Algorithm 14), μ_ℓ (Algorithm 15), and τ_ℓ (Algorithm 16) empirically regain the optimal order of convergence. The error curves over $N=\mathcal{T}_\ell$ almost coincide in any case. Whereas μ_ℓ is attractive in practice since there is almost no implementational overhead, we found that the ϱ_ℓ-based strategy is favorable for larger problems with respect to computational time. We therefore recommend to use μ_ℓ to set-up an adaptive scheme and check the implementation, while ϱ_ℓ should be implemented to obtain the most effective realization.

5.3. Generalization to 3D

Similar arguments can be used to prove that the main results in Theorems 4, 6, 10, and 12 remain valid if we consider the

model problem (1) and its FEM–BEM formulation (2) in 3D. The only critical difference is that an approximation result of [14,30] is needed to localize the $H^{1/2}$-norm in (26), since H^1-functions on 2D manifolds can be discontinuous. Then, the arclength derivative $(\cdot)'$ has to be replaced by the surface gradient $\nabla_\Gamma(\cdot)$.

The localization of the $H^{1/2}$-norm for the data approximation, cf. Proposition 2, is currently under consideration [38]. Since H^1-functions on the 2D manifold Γ can be discontinuous, nodal interpolation I_ℓ must not be used to discretize $U_{0,\ell}=I_\ell u_0$. Instead, we prove in [38] that one may use either the L^2-orthogonal projection onto $\mathcal{S}^1(\mathcal{E}_\ell^\Gamma)$ or a Scott–Zhang-type quasi-interpolation operator. Similar to the 2D case, the data approximation term then reads $\mathrm{osc}_\ell=\|h_\ell^{1/2}\nabla_\Gamma(u_0-U_{0,\ell})\|_{L^2(\Gamma)}$. Corollaries 5, 7, and 11 then hold accordingly.

5.4. Open questions and future work

Mathematically, not much is known about the convergence of the proposed adaptive algorithms in the sense of $\mathbf{U}_\ell\to\mathbf{u}$ as $\ell\to\infty$. For efficient estimators like μ_ℓ and τ_ℓ, convergence of the estimator to zero is a necessary condition. Based on the concept of estimator reduction [3], it is proven in [5] that the $(h-h/2)$-based Algorithm 15 leads to estimator convergence $\overline{\mu}_\ell\to 0$ as $\ell\to\infty$. To the best of our knowledge, there are no convergence results known for the other two adaptive algorithms which are driven by ϱ_ℓ resp. τ_ℓ.

Moreover, quasi-optimality of all three algorithms which is empirically observed in numerical experiments, is mathematically open. Recently, there has been a huge step in the analytical understanding of convergence and quasi-optimality of adaptive finite element methods, cf. [21] and the references therein. However, even for simple model problems, quasi-optimality of adaptive boundary element methods is a major open issue, cf. [3,18,31].

In our numerical experiments, we empirically observe that adaptive mesh-refinement leads to the optimal order of convergence in each component of the error of the Galerkin solution $\mathbf{U}_\ell=(U_\ell,\Phi_\ell)\in\mathcal{X}_\ell$, i.e. $\|u-U_\ell\|_{H^1(\Omega)}=\mathcal{O}(N^{-1/2})$ and $\|\phi-\Phi_\ell\|_{H^{-1/2}(\Gamma)}=\mathcal{O}(N^{-3/4})$, which is observed for all adaptive strategies in Figs. 3–5. In fact, the quasi-optimality (11) would only predict $\mathcal{O}(N^{-1/2})$ for both terms, if this rate is possible. To the best of our knowledge, this observation is not even mathematically understood in case of a smooth solution $\mathbf{u}=(u,\phi)\in H^2(\Omega)\times H^1(\Gamma)\subset\mathcal{H}$ and uniform mesh-refinement.

Finally, the saturation assumption (31) is mathematically open. In case of finite element model problems, one can prove that small data oscillation implies the saturation assumption [26]. More precisely, the triangulation has to resolve the given data so that the data approximation error is smaller than the Galerkin error. One may expect that a similar result should also hold for BEM or the FEM–BEM coupling. The non-locality of the involved boundary integral operators imposes, however, severe difficulties, and we expect that new mathematical techniques have to be developed. Anyhow, this is an additional reason why one should include the resolution of the given data into the adaptive scheme.

Acknowledgments

The research of the authors is supported through the FWF project *Adaptive Boundary Element Method*, funded by the Austrian Science Fund (FWF) under Grant P21732.

References

[1] Ainsworth M, Oden JT. A posteriori error estimation in finite element analysis. New-York: Wiley-Interscience; 2000.
[2] Aurada M, Ebner M, Ferraz-Leite S, Mayr M, Goldenits P, Karkulik M, et al. HILBERT—A MATLAB implementation of adaptive BEM. ASC Report 44/2009. Wien: Institute for Analysis and Scientific Computing, Vienna University of Technology; 2009, software download at ⟨http://www.asc.tuwien.ac.at/abem/hilbert/⟩.
[3] Aurada M, Ferraz-Leite S, Praetorius D. Estimator reduction and convergence of adaptive FEM and BEM, Appl Numer Math, doi:10.1016/j.apnum.2011.06.014. In press.
[4] Aurada M, Feischl M, Karkulik M, Praetorius D. A posteriori error estimates for the Johnson–Nédélec FEM–BEM coupling. ASC Report 18/2011. Wien: Institute for Analysis and Scientific Computing, Vienna University of Technology; 2011.
[5] Aurada M, Feischl M, Praetorius D. Convergence of some adaptive FEM–BEM coupling. ASC Report 06/2010. Wien: Institute for Analysis and Scientific Computing, Vienna University of Technology; 2010.
[6] Aurada M, Goldenits P, Praetorius D. Convergence of data perturbed adaptive boundary element methods. ASC Report 40/2009. Wien: Institute for Analysis and Scientific Computing, Vienna University of Technology; 2009.
[7] Bank R. Hierarchical bases and the finite element method. Acta Numer 1996;5:1–45.
[8] Bank R, Smith R. A posteriori error-estimates based on hierarchical bases. SIAM J Numer Anal 1993;30:921–35.
[9] Bank R, Weiser A. Some a posteriori error estimators for elliptic partial differential equations. Math Comput 1985;44:283–301.
[10] Bornemann F, Erdmann B, Kornhuber R. A-posteriori error-estimates for elliptic problems in 2 and 3 space dimensions. SIAM J Numer Anal 1996;33:1188–204.
[11] Carstensen C. A posteriori error estimate for the symmetric coupling of finite elements and boundary elements. Computing 1996;57:301–22.
[12] Carstensen C. An a posteriori error estimate for a first-kind integral equation. Math Comput 1997;66:139–55.
[13] Carstensen C, Faermann B. Mathematical foundation of a posteriori error estimates and adaptive mesh-refining algorithms for boundary integral equations of the first kind. Eng Anal Bound Elem 2001;25:497–509.
[14] Carstensen C, Maischak M, Stephan E. A posteriori error estimate and h-adaptive algorithm on surfaces for Symm's integral equation. Numer Math 2001;90:197–213.
[15] Carstensen C, Praetorius D. Averaging techniques for the effective numerical solution of Symm's integral equation of the first kind. SIAM J Sci Comput 2006;27:1226–60.
[16] Carstensen C, Praetorius D. Averaging techniques for the a posteriori BEM error control for a hypersingular integral equation in two dimensions. SIAM J Sci Comput 2007;29:782–810.
[18] Carstensen C, Praetorius D. Convergence of adaptive boundary element methods. ASC Report 15/2009. Wien: Institute for Analysis and Scientific Computing, Vienna University of Technology; 2009.
[19] Chernov A, von Petersdorff T, Schwab C. Exponential convergence of hp quadrature for integral operators with gevrey kernels. Technical Report 2009-03, ETH Zürich; January 2009.
[20] Carstensen C, Stephan E. Adaptive coupling of boundary elements and finite elements. Math Model Numer Anal 1995;29:779–817.
[21] Cascon J, Kreuzer C, Nochetto R, Siebert K. Quasi-optimal convergence rate for an adaptive finite element method. SIAM J Numer Anal 2008;46:2524–50.
[22] Costabel M. A symmetric method for the coupling of finite elements and boundary elements. In: Whiteman J, editor. The mathematics of finite elements and applications IV, MAFELAP 1987. London: Academic Press; 1988. p. 281–8.
[23] Costabel M, Ervin V, Stephan E. Experimental convergence rates for various couplings of boundary and finite elements. Math Comput Modelling 1991;15:93–102.
[24] Costabel M, Stephan E. Coupling of finite and boundary element methods for an elasto-plastic interface problem. SIAM J Numer Anal 1990;27:1212–26.
[25] Dörfler W. A convergent adaptive algorithm for Poisson's equation. SIAM J Numer Anal 1996;33:1106–24.
[26] Dörfler W, Nochetto R. Small data oscillation implies the saturation assumption. Numer Math 2002;91:1–12.
[27] Erath C, Ferraz-Leite S, Funken S, Praetorius D. Energy norm based a posteriori error estimation for boundary element methods in two dimensions. Appl Numer Math 2009;59:2713–34.
[28] Erath C, Funken S, Goldenits P, Praetorius D. Simple error estimators for the Galerkin BEM for some hypersingular integral equation in 2D. ASC Report 20/2009. Wien: Institute for Analysis and Scientific Computing, Vienna University of Technology; 2009.
[29] Faermann B. Localization of the Aronszajn–Slobodeckij norm and application to adaptive boundary element methods. I. The two-dimensional case. IMA J Numer Anal 2000;20:203–34.
[30] Faermann B. Localization of the Aronszajn-Slobodeckij norm and application to adaptive boundary element methods. II. The three-dimensional case. Numer Math 2002;92:467–99.
[31] Ferraz-Leite S, Ortner C, Praetorius D. Convergence of simple adaptive Galerkin schemes based on $h-h/2$ error estimators. Numer Math 2010;116:291–316.
[32] Ferraz-Leite S, Praetorius D. Simple a posteriori error estimators for the h-version of the boundary element method. Computing 2008;83:135–62.
[33] Feischl M, Page M, Praetorius D. Convergence and quasi-optimality of adaptive FEM with inhomogeneous Dirichlet data. ASC Report 34/2010. Wien: Institute for Analysis and Scientific Computing, Vienna University of Technology; 2010.

[34] Gatica G, Wendland W. Coupling of mixed finite elements and boundary elements for linear and nonlinear elliptic problems. Appl Anal 1996;63:39–75.
[35] Hairer E, Nørsett S, Wanner G. Solving ordinary differential equations I. Nonstiff problems. New York: Springer; 1987.
[36] Hsiao G. The coupling of boundary element and finite element methods. ZAMM Z Angew Math Mech 1990;70:493–503.
[37] Johnson J, Nédélec JC. On the coupling of boundary integral and finite element methods. Math Comput 1980;35:1063–79.
[38] Karkulik M, Praetorius D. Convergence of adaptive 3D BEM for weakly singular integral equations based on isotropic mesh-refinement, work in progress.
[39] Krebs A, Maischak M, Stephan E. Adaptive FEM–BEM coupling with a Schur complement error indicator. Appl Numer Math 2010;60:798–808.
[41] McLean W. Strongly elliptic systems and boundary integral equations. Cambridge: Cambridge University Press; 2000.
[42] Mund P, Stephan E. An additive two-level method for the coupling of nonlinear FEM–BEM equations. SIAM J Numer Anal 1999;36:1001–21.
[43] Rjasanov S, Steinbach O. The fast solution of boundary integral equations. New York: Springer; 2007.
[44] Sauter S, Schwab C. Randelementmethoden: analyse, Numerik und Implementierung schneller Algorithmen. Wiesbaden: Teubner Verlag; 2004. [in German].
[45] Schwab C. Variable order composite quadrature of singular and nearly singular integrals. Computing 1994;53.
[46] Sayas F-J. The validity of Johnson–Nédélec's BEM–FEM coupling on polygonal interfaces. SIAM J Numer Anal 2009;47:3451–63.
[47] Stephan E, Suri M. The hp-version of the boundary element method on polygonal domains with quasiuniform meshes. Math Modelling Numer Anal 1991;25:783–807.
[49] Verfürth R. A review of a posteriori error estimation and adaptive mesh-refinement techniques. Stuttgart: Teubner; 1996.
[50] Yserentant H. On the multi-level splitting of finite element spaces. Numer Math 1986;49:379–412.